A Quantile-based Sequential Approach to Reliability-based Design Optimization via Error-controlled Adaptive Kriging

Chi Zhang* and Abdollah Shafieezadeh**
The Ohio State University, Columbus, OH 43210 USA

Abstract

A significant challenge with reliability-based design optimization (RBDO) is the high computational cost associated with the double-loop structure that entails a large number of function calls for both the optimization process and reliability analysis. Several decoupling methods have been developed to improve the efficiency of RBDO. In addition, surrogate models have been used to replace the original time-consuming models and improve the computational efficiency. This paper proposes a novel quantile-based sequential RBDO method using Kriging surrogate models for problems with independent constraint functions. An error-controlled adaptive Kriging scheme is integrated to derive accuracy information of surrogate models and develop a strategy that facilitates independent training of the models for the performance function. The proposed independent training avoids unnecessary performance function evaluations while ensuring the accuracy of reliability estimates. Moreover, a new sampling approach is proposed that allows refinement of surrogate models for both deterministic and probabilistic constraints. Five numerical examples are carried out to demonstrate the performance of the proposed method. It is observed that the proposed method is able to converge to the optimum design with significantly fewer function evaluations than the state-of-the-art methods based on surrogate models given the constraint functions are independent.

Key words: RBDO; Adaptive Kriging; Surrogate model; Reliability analysis; Sampling strategy; Error control

1. Introduction

Deterministic design optimization (DDO) provides the optimum design of structures and systems while satisfying some performance constraints without considering uncertainties. A typical DDO problem is often formulated as follows:

$$\begin{aligned} & & find.\, \boldsymbol{d} \\ & & min.\,\, J(\boldsymbol{d}) \\ s.\,t.\,\, g_i(\boldsymbol{d}) \leq 0, i = 1, 2, \dots, m \\ & \boldsymbol{d}^l \leq \boldsymbol{d} \leq \boldsymbol{d}^u \end{aligned} \tag{1}$$

where $J(\cdot)$ and $g_i(\cdot)$ are the objective function and the i_{th} performance function, respectively, \boldsymbol{d} is the vector of design variables, m is the number of constraints, and \boldsymbol{d}^l and \boldsymbol{d}^u are the lower and upper bound vector of design variables, respectively. The feasible region is defined as $g_i(\boldsymbol{d}) \leq 0$, i.e., the failure occurs when the limit state function $g_i(\boldsymbol{d})$ is positive. Note that in some literature, the sign convention could be the opposite.

However, there are large uncertainties in many phenomena of practical engineering, including many variabilities in the fabrication processes and operation conditions (Liu et al., 2018b, 2020). The uncertainties can cause the unreliability of the optimal design yielded by DDO. On the other hand, reliability-based design optimization (RBDO) accounts for the variations of the performance induced by the uncertainties and therefore is able to find optimal solutions that are reliable. A typical RBDO problem can be formulated as follows:

$$find. \mathbf{d}, \boldsymbol{\mu}_{x}$$

$$min. J(\mathbf{d}, \boldsymbol{\mu}_{x}, \boldsymbol{\mu}_{p})$$

$$s.t. Pr (g_{i}(\mathbf{d}, x, p) > 0) \leq \Phi(-\beta_{i}^{t}), i = 1, 2, ..., m$$

$$\mathbf{d}^{l} \leq \mathbf{d} \leq \mathbf{d}^{u}, \boldsymbol{\mu}_{x}^{l} \leq \boldsymbol{\mu}_{x} \leq \boldsymbol{\mu}_{x}^{u}$$

$$(2)$$

where d is the deterministic design vector, x and p are the random design and parameter vectors with the mean of μ_x and μ_p , respectively and $Pr(g_i(\cdot) > 0)$ is the probability that the i_{th} performance function $g_i(\cdot)$ is violated. $\Phi(-\beta_i^t)$ is the target failure probability for the i_{th} constraint where $\Phi(\cdot)$ is the standard normal cumulative density function (CDF) and β_i is the i_{th} target reliability index. μ_x^l and μ_x^u are the lower and upper bound vector of the mean of the random design variables, respectively.

RBDO intrinsically involves a double loop structure that contains an outer loop of DDO and an inner loop of reliability analysis due to the nature of the probabilistic constraints. There are two main approaches for dealing with the probabilistic constraints: reliability index approach (RIA) (Tu et al., 1999) and performance measure approach (PMA) (Tu et al., 1999). RIA takes the probabilistic constraint in the format of reliability index. PMA, on the other hand, uses an inverse transformation of constraints in RIA. It has been found that PMA tends to be more robust and converge faster compared to RIA (Lee et al., 2002; Ramu et al., 2006; Tu et al., 1999; Valdebenito and Schuëller, 2010). Many methods are proposed to deal with the optimization problem in PMA, such as Advanced Mean Value (AMV) method (Wu, 1994; Wu et al., 1990), Conjugate Mean Value (CMV) method and Hybrid Mean Value (HMV) method (Youn et al., 2003). However, the double loop or nested structure in both PMA and RIA renders some RBDO problems extremely computationally demanding. This challenge arises as reliability analyses, which are often time consuming, are required in each iteration of the optimization process. Many methods have been developed to deal with the high computational burden of RBDO problems. Chen et al. (1997) converted the double loop structure into a single loop single structure by replacing the probabilistic constraint with an approximate deterministic constraint based on the value of the design variables. Wu et al. (2001) proposed the safety-factor approach that uses approximately equivalent deterministic constraints for RBDO problems. Du and Chen (2004) proposed the well-known sequential optimization and reliability assessment (SORA) where the deterministic constraints are shifted towards the probabilistic constraints progressively by the amount determined by the inverse most probable points (iMPPs). Yang and Gu (2004) found that SORA and SFA are conceptually identical and work identically in the standard normal space. Koch et al. (2004) proposed the approximate moment approach (AMA) that also transforms the probabilistic constraints to approximated deterministic constraint via Taylor series expansion at the mean values. Yi et al. (2016) proposed an efficient approximate sequential optimization reliability assessment (ASORA) method based on SORA. These methods all improve the efficiency of RBDO, although they usually entail some degree of simplification of the performance functions, and therefore introduce approximation errors.

In RBDO problems, function calls, which could be required many times by both reliability analysis and optimization process, often entail time-consuming model evaluations especially for problems that involve high-fidelity finite element models. Even with the aforementioned methods developed to improve the efficiency of RBDO, the number of function calls can still be formidable when the model evaluations are highly expensive. In recent years, surrogate models are used to replace the time-consuming original models to improve the efficiency of reliability analysis as well as RBDO. Many surrogate models or meta-models can be used for this purpose, among which Polynomial Response Surface (Giunta et al., 2006; Romero et al., 2004; Zhao et al., 2017), Polynomial Chaos Expansion (PCE) (Blatman and Sudret, 2010), Support Vector Regression (SVR) (Bourinet, 2016; Dai et al., 2012), Radial Basis Function (RBF) (Li et al., 2020) and Kriging (Bichon et al., 2008; Dubourg et al., 2011; Echard et al., 2011; Li et al., 2019; Moustapha et al., 2016; Song et al., 2019; Wang and Shafieezadeh, 2019; Zhang et al., 2020) are the most popular. Kriging, due to its ability to provide estimates of the expected model response and the associated variance, has gained significant popularity. Kriging-based reliability methods such as Efficient Global Reliability Analysis (EGRA) (Bichon et al., 2008) and Active learning reliability method combining Kriging and Monte Carlo Simulation (AK-MCS) (Echard et al., 2011) have utilized

these features to locate the next "best" training points and adaptively build surrogate models, starting the trend of using Kriging in reliability analysis (Echard et al., 2013; Fauriat and Gayton, 2014; Huang et al., 2016; Lv et al., 2015; Wang and Shafieezadeh, 2019, 2018). In the area of RBDO, there are also numerous Kriging-based methods, some of which are reviewed here. Mourelatos (2005) leveraged optimal Latin hypercube sampling and Kriging model for a RBDO of crankshaft main bearings. Pretorius et al. (2004) used Kriging and HMV to solve a continuous casting design optimization problem. Lee and Jung (2008) proposed a sampling technique named constraint boundary sampling (CBS) to improve the accuracy and efficiency of Kriging-based RBDO. Lee at al. (2011) presented a sampling-based RBDO approach using Kriging and a stochastic sensitivity analysis. Dubourg et al. (2011) developed a strategy to solve RBDO problems with the Kriging surrogate models built in so-called augmented reliability space and subset simulation. Zhuang and Pan (2012) proposed an expected relative improvement (ERI) sampling criterion and used it to construct surrogate models for SORA. Bichon et al. (2012) investigated the use of the efficient global optimization (EGO) and EGRA to construct Kriging surrogate models for RBDO problems. Inspired by CBS, Chen et al. (2015) proposed an importance boundary sampling (IBS) method to enhance the efficiency of RBDO. Moustapha et al. (2016) proposed a quantile-based, conservative optimization procedure for structures in an uncertain environment using Kriging surrogate models. Liu et al. (2017) proposed an adaptive local range sampling method for RBDO using SVR and Kriging. Inspired by SORA, Li et al. (2019) and Li et al. (2020) proposed similar quantile-based sequential optimization methods using RBF and Kriging, respectively. In both methods, computationally cheap surrogate models are used. The reduced cost of function evaluations allows the estimation of quantile of the target failure probabilities, which can be used as the shift from the deterministic constraints to probabilistic constraints. Both methods showed their accuracy and efficiency through numerical examples. However, the stopping criterion used in both methods are not directly related to the accuracy of reliability analysis. In addition, the training points are shared among different constraint functions, introducing unnecessary model evaluations when the constraint functions are independent from each other. For instance, in the studies of transmission line systems, the conductors and the tower can have separate high-fidelity finite element models that can be analyzed independently (Darestani et al., 2020; Ma et al., 2020).

In order to address these gaps, this paper proposes a quantile-based sequential RBDO method using independent training with error-controlled adaptive kriging and a novel sampling approach. The proposed method aims to solve RBDO problems with independent performance functions. In the proposed method, the maximum error rates of the surrogate models for constraint functions are derived to measure the accuracy of the models for reliability analysis. This error information also allows the surrogate models of different constraint functions to be trained independently, avoiding unnecessary evaluations of models while ensuring the accuracy of the surrogate models. In addition, a sampling strategy facilitated by the independent training is proposed to improve the construction of surrogate models for constraint functions. The sampling approach selects training points considering refining the models on both deterministic and probabilistic constraints, of which the latter is often not considered in existing sampling approaches. The performance of the proposed method is demonstrated via five numerical examples.

This paper consists of six sections. In Section 2, a review of commonly used RBDO methods is given. In Section 3, the adaptive Kriging method and the error-based stopping criterion are presented. Next in Section 4, a new sampling approach is proposed, and its integration along with error-based stopping criterion into RBDO and the overall structure of the proposed method are elaborated. In Section 5, five numerical examples are carried out to demonstrate the efficiency and accuracy of the proposed method. Conclusions are drawn in Section 6.

2. Typical RBDO Methods

This section presents an overview of commonly used RBDO methods.

2.1 RIA

In RIA, reliability indexes are used to represent the probabilistic constraints of RBDO. The formulation of RBDO in RIA is as follows:

$$find. \mathbf{d}, \boldsymbol{\mu}_{x}$$

$$min. J(\mathbf{d}, \boldsymbol{\mu}_{x}, \boldsymbol{\mu}_{p})$$

$$s.t. \beta_{i} \geq \beta_{i}^{t}, i = 1, 2, ..., m$$

$$\mathbf{d}^{l} \leq \mathbf{d} \leq \mathbf{d}^{u}, \boldsymbol{\mu}_{x}^{l} \leq \boldsymbol{\mu}_{x} \leq \boldsymbol{\mu}_{x}^{u}$$

$$(3)$$

 $d^l \leq d \leq d^u, \mu_x{}^l \leq \mu_x \leq \mu_x{}^u$ where β_i is the i_{th} reliability index for performance function g_i corresponding to $[d, \mu_x, \mu_p]$, which can be acquired by solving the sub-optimization problem formulated as follows:

$$min. \beta_i = ||\mathbf{U}||$$
s. t. $G_i(\mathbf{d}, \mathbf{U}) = 0$ (4)

where U is the independent standard normal random variable vectors corresponding to the original random variable vector $\mathbf{x}^t = [\mathbf{x}, \mathbf{p}]$, and G_i is the probabilistic constraint, i.e., $G_i(\mathbf{d}, \mathbf{U}) =$ $g_i(\boldsymbol{d},\boldsymbol{x},\boldsymbol{p})$. The sub-optimization problem can be solved using the Hasofer-Lind and Rackwitz-Fiessler (HL-RF) method (Hasofer and Lind, 1974; Liu and Der Kiureghian, 1991).

2.2 PMA

In contrast to RIA, PMA uses an inverse transformation of constraints in RIA

find.
$$d, \mu_x$$
min. $J(d, \mu_x, \mu_p)$

s. t. $G_i^* \ge 0, i = 1, 2, ..., m$

$$d^l \le d \le d^u, \mu_x^l \le \mu_x \le \mu_x^u$$
where G_i^* is the maximum of the performance function with respect to the points that have the target

reliability index, which is the solution to the following sub-optimization problem:

$$G_i^* = max(G_i(\boldsymbol{d}, \boldsymbol{U}))$$

$$s.t. \ ||\boldsymbol{U}|| = \beta_i^t$$
(6)

The sub-optimization can be solved using the AMV method (Wu, 1994; Wu et al., 1990), CMV method and HMV method (Youn et al., 2003).

Both RIA and PMA are based on the computationally costly double-loop structure. Many methods are developed to convert the double-loop into a single loop or a serial loop. Some of these decoupling methods are introduced in the next sub-section.

2.3 Decoupling methods

Decoupling methods convert the double-loop structure into a serial loop structure. In this subsection, the commonly used decouple method, SORA, is introduced followed by the quantilebased methods with surrogate models.

2.3.1 **SORA**

Du and Chen (2004) proposed SORA that transforms the double loop structure into sequence of deterministic optimizations and reliability analyses. In each iteration, a deterministic optimization and reliability analyses are performed. The reliability analyses provide the most probable points (MPPs) that can be used to calculate the shift, which are subsequently used to convert the deterministic constraints to probabilistic constraints. The RBDO problem using SORA can be formulated as follows:

$$find. \, \mathbf{d}, \mu_{x} min. \, J(\mathbf{d}, \mu_{x}, \mu_{p}) s.t. \, G_{i}(\mathbf{d}, \mu_{x} - s_{x}^{(k)}, \mu_{p} - s_{p}^{(k)}) \ge 0, i = 1, 2, ..., m \mathbf{d}^{l} \le \mathbf{d} \le \mathbf{d}^{u}, \mu_{x}^{l} \le \mu_{x} \le \mu_{x}^{u}$$

$$(7)$$

where $s_x^{(k)}$ and $s_p^{(k)}$ are shift value vectors for random variable x and p, respectively, in k_{th}

$$\left(s_{x}^{(k)}, s_{p}^{(k)}\right) = \left(\mu_{x}^{(k-1)}, \mu_{p}\right) - \left(x_{MPP}^{(k-1)}, p_{MPP}^{(k-1)}\right)$$
 (8)

iteration. They can be obtained using the following equation: $(s_x^{(k)}, s_p^{(k)}) = (\mu_x^{(k-1)}, \mu_p) - (x_{MPP}^{(k-1)}, p_{MPP}^{(k-1)})$ (8) where $\mu_x^{(k-1)}$ is the optimal point in the $(k-1)_{th}$ iteration, $x_{MPP}^{(k-1)}$ is the vector corresponding to x of MPPs in the original design space in $(k-1)_{th}$ iteration, and $p_{MPP}^{(k-1)}$ is the vector corresponding to p of MPPs in the original design space in the $(k-1)_{th}$ iteration. In SORA, MPPs can be obtained by solving the sub-optimization problem in PMA (Eq. (6)). The shift for a simple 2D example is depicted in Fig. 1. As shown in this figure, in every iteration, the constraints are shifted closer towards the actual probabilistic constraints. The flowchart of SORA is summarized in Fig. 2.

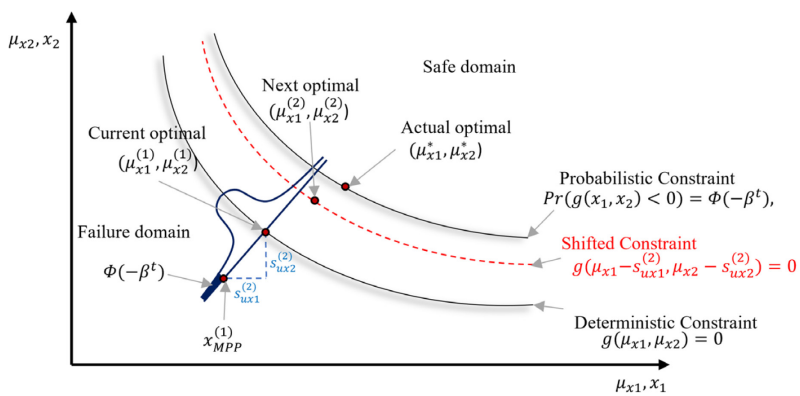


Fig.1 Constraint shift in SORA

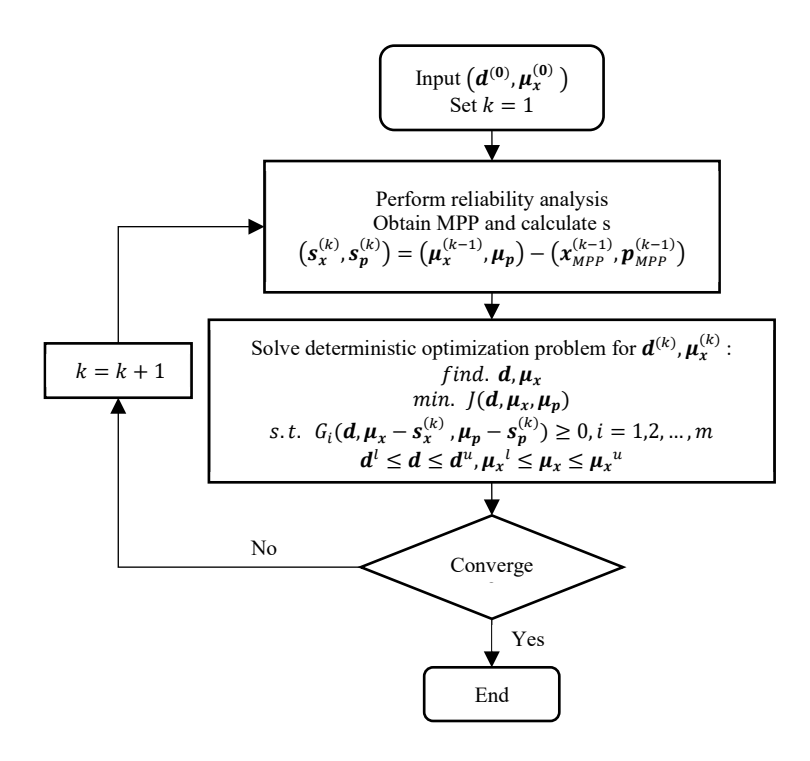


Fig.2 Flowchart of SORA

SORA decouples the double loop structure to improve the efficiency, however, it is based on MPPs, which are imaginary points that may not truly reflect the reliability of the structure or system. In the next sub-section, the quantile-based methods, which are similar to SORA yet independent of MPPs, are introduced.

2.3.2 Quantile-based methods with surrogate models

Inspired by SORA, Li et al. (2019) and Li et al. (2020) proposed the quantile-based sequential methods with RBF and Kriging, respectively. The surrogate models, which are significantly cheaper to evaluate, allow leveraging Monte Carlo Simulation (MCS) for reliability analysis. Instead of using MPP-based shifts, they utilize the shifts calculated by MCS. Thus, the error introduced by the approximation in MPP is eliminated and only the error introduced by the surrogate models is of concern. The RBDO problem using the quantile-based method is formulated as follows:

$$find. \mathbf{d}, \boldsymbol{\mu}_{x}$$

$$min. J(\mathbf{d}, \boldsymbol{\mu}_{x}, \boldsymbol{\mu}_{p})$$

$$s. t. g_{i}(\mathbf{d}, \boldsymbol{\mu}_{x}, \boldsymbol{\mu}_{p}) + c_{i}^{(k)} > 0, i = 1, 2, ..., m$$

$$\mathbf{d}^{l} \leq \mathbf{d} \leq \mathbf{d}^{u}, \boldsymbol{\mu}_{x}^{l} \leq \boldsymbol{\mu}_{x} \leq \boldsymbol{\mu}_{x}^{u}$$

$$(9)$$

where $c_i^{(k)}$ is the shift for i_{th} deterministic constraint in k_{th} iteration and it can be calculated using the following equation:

$$c_i^{(k)} = CDF^{-1}(\Phi(\beta_i^t)|g_i) - g_i(\mathbf{d}^{(k-1)}, \boldsymbol{\mu}_x^{(k-1)}, \boldsymbol{\mu}_p)$$
 (10)

where $d^{(k-1)}$ is the optimal deterministic design variable in the $(k-1)_{th}$ iteration, $CDF^{-1}(\Phi(\beta_i^t)|g_i)$ is the inverse cumulative distribution function (CDF) with respect to target reliability $\Phi(\beta_i^t)$ for g_i , which corresponds to the quantile of the target reliability. The inverse CDF can be determined by fitting a distribution to a population of MCS. This type of fitting problem can be solved using techniques in Li et al. (2018a, 2018c), in this paper, fitdist in MATLAB is used to fit the distribution. The MCS population requires a large number of function evaluations, which are possible thanks to the utilization of the surrogate models. The main idea of the quantile-based sequential methods is quite similar to SORA, where the constraints are shifted towards the probabilistic constraints gradually. However, instead of shifting the constraints through design variables, it shifts the constraints through offsets $c_i^{(k)}$ on constraint functions. The shift for a simple 2D example using the methods is depicted in Fig. 3. An offset is applied to the constraint for the purpose of shifting. In these methods, the surrogate model is refined adaptively during the sequential optimization process. The approaches in Li et al. (2019) and Li et al. (2020) can be both summarized in the flowchart in Fig. 4. Note that the surrogate model in dashed box is exclusive in Li et al. (2020), as only Kriging can provide uncertainty information that helps the identification of the next "best" training points. Both methods use the aforementioned process and adaptively enrich the surrogate models sequentially during the process of RBDO.

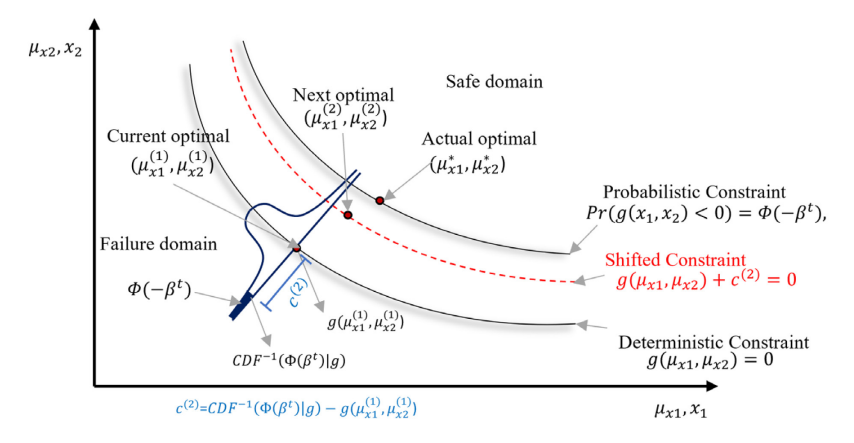


Fig. 3 Constraint shift in quantile-based sequential optimization

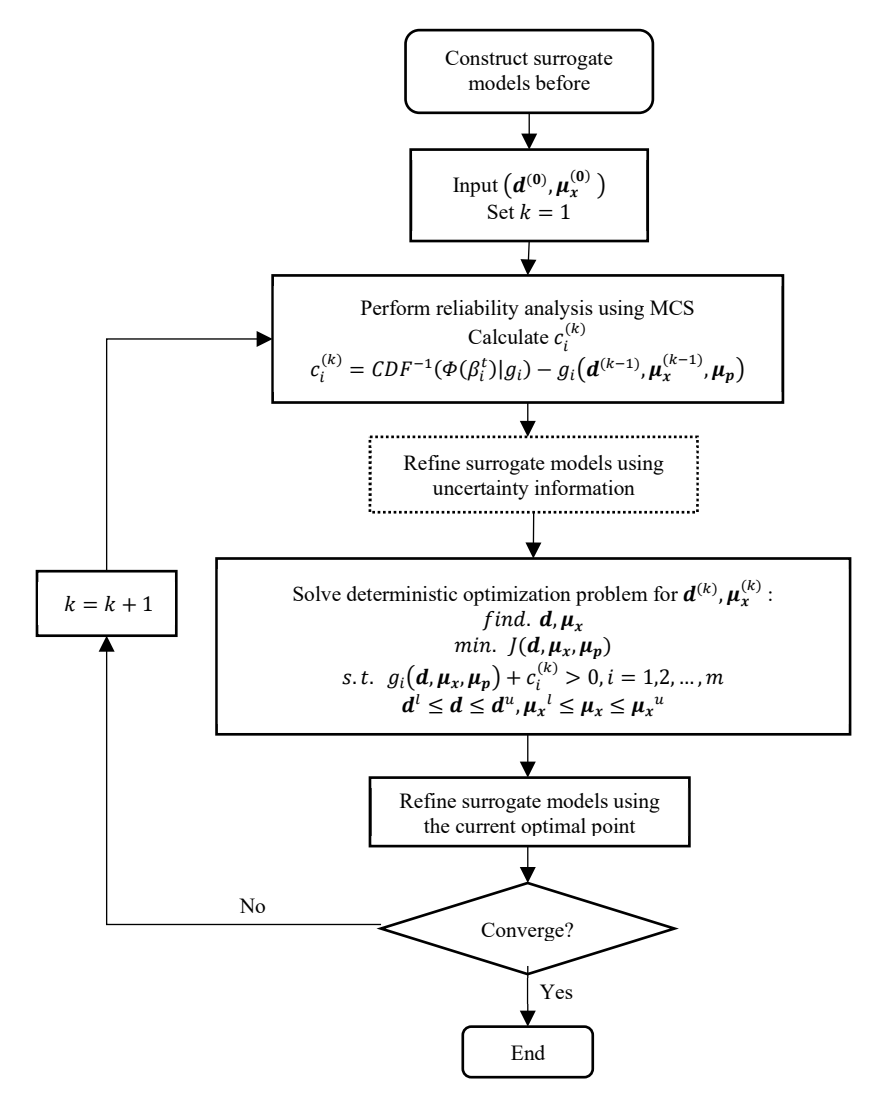


Fig.4 Flowchart of quantile-based sequential optimization

Li et al. (2019) initialized the RBF surrogate models with $(2n_d + 1)$ points obtained via Latin Hypercube sampling (LHS), where n_d is the dimension of the design variables, and then added results of the deterministic optimization as the training points until some convergence requirement is met. Then the method enters the process of Eq. (9) using the constructed surrogate model and the current optimal point is added as the training point in each iteration until the shift converges. The use of the current optimal point as the training point may lead to local optima or inaccurate surrogate models which cannot represent the true reliability of the structure or system. In addition, RBF cannot provide the uncertainty information as Kriging to instruct the construction of the surrogate model. Li et al. (2020), on the other hand, used the Kriging surrogate model and took advantage of the uncertainty information. They used LHS to get $5n_d$ or $10n_d$ initial training points and then entered the process of Eq. (9) directly. In the optimization process, they refined the Kriging surrogate model by adding both the current optimal points and a point informed by the uncertainty information. In Li et al. (2020), all performance functions share the same training points, which may result in unnecessary or ineffective training for some performance functions in problems with independent performance functions. In addition, the accuracy of surrogate constraints in terms of the reliability is not known. Hence, we propose a new quantile-based method with adaptive Kriging to tackle these problems. In the next section, an overview of Kriging and an error-based stopping criterion are presented.

3. Adaptive Kriging Method

As mentioned in Section 1, Kriging surrogate models are commonly used in reliability analysis and RBDO. In this section, a review of Kriging surrogate models is given first as follows.

3.1 Kriging surrogate model

Let $g(X_g)$ denote the original model with variables X_g , which contains all the variables including both deterministic and random variables in the problem. The stochastic estimator of $g(X_g)$ based on Kriging shown by $\hat{g}(X_q)$ can be formulated as follows:

$$\widehat{g}(\mathbf{X}_g) = F(\boldsymbol{\beta}, \mathbf{X}_g) + \mathcal{G}_{\mathcal{P}}(\mathbf{X}_g) = \boldsymbol{\beta}^T f(\mathbf{X}_g) + \mathcal{G}_{\mathcal{P}}(\mathbf{X}_g)$$
(11)

where x_q is the vector of random variables, $F(\beta, x_q)$ are regression elements, and $gp(x_q)$ is a Gaussian process. $F(\beta, x_q)$ is the product of $f(x_q)$, which is the Kriging basis, and β , which is the corresponding set of coefficients. The Gaussian process $gp(x_q)$ has a zero mean and a covariance matrix. The covariance matrix can be formulated as: $COV\left(gp\left(\boldsymbol{x}_{g}^{(i)}\right),gp\left(\boldsymbol{x}_{g}^{(j)}\right)\right)=\sigma^{2}R\left(\boldsymbol{x}_{g}^{(i)},\boldsymbol{x}_{g}^{(j)};\boldsymbol{\theta}\right)$

$$COV\left(gp\left(\mathbf{x}_{g}^{(i)}\right), gp\left(\mathbf{x}_{g}^{(j)}\right)\right) = \sigma^{2}R\left(\mathbf{x}_{g}^{(i)}, \mathbf{x}_{g}^{(j)}; \boldsymbol{\theta}\right)$$
(12)

where σ^2 is the process variance or the generalized mean square error (MSE) from the regression, $x_g^{(i)}$ and $x_g^{(j)}$ are any two observations, and $R\left(x_g^{(i)}, x_g^{(j)}; \boldsymbol{\theta}\right)$ is the kernel function parametrized by $\boldsymbol{\theta}$, it represents the correlation between observations $\boldsymbol{x}_g^{(i)}$ and $\boldsymbol{x}_g^{(j)}$. The Gaussian kernel function is used in this study, which can be formulated as:

$$R\left(\mathbf{x}_{g}^{(i)}, \mathbf{x}_{g}^{(j)}; \boldsymbol{\theta}\right) = \prod_{k=1}^{N} exp\left(-\theta^{k} \left(x_{g_{k}}^{(i)} - x_{g_{k}}^{(j)}\right)^{2}\right)$$
(13)

where $x_{g_k}^{(i)}$ is the k_{th} dimension of $x_g^{(i)}$ and $\boldsymbol{\theta}$ can be estimated via the Maximum Likelihood Estimation (MLE) method via the DACE toolbox (Lophaven et al., 2002a, 2002b). The formulation based on MLE is as follows:

$$\boldsymbol{\theta}^* = \underset{\boldsymbol{\theta}}{\operatorname{argmin}} \left(\left| \boldsymbol{R} \left(\boldsymbol{x}_g^{(i)}, \boldsymbol{x}_g^{(j)}; \boldsymbol{\theta} \right) \right|^{\frac{1}{m}} \sigma^2 \right)$$
 (14)

where m is the number of training points. The regression coefficients β , and the predicted mean and variance can be then determined as follows ("UQLab Kriging (Gaussian process modelling) manual," 2017):

$$\boldsymbol{\beta} = (\boldsymbol{F}^{T} \boldsymbol{R}^{-1} \boldsymbol{F})^{-1} \boldsymbol{F}^{T} \boldsymbol{R}^{-1} \boldsymbol{Y}$$

$$\mu_{\hat{g}}(\boldsymbol{x}_{g}) = \boldsymbol{f}^{T}(\boldsymbol{x}_{g}) \boldsymbol{\beta} + \boldsymbol{r}^{T}(\boldsymbol{x}_{g}) \boldsymbol{R}^{-1} (\boldsymbol{y} - \boldsymbol{F} \boldsymbol{\beta})$$

$$\sigma_{\hat{g}}^{2}(\boldsymbol{x}_{g}) = \sigma^{2} - \sigma^{2} \boldsymbol{r}^{T}(\boldsymbol{x}_{g}) \boldsymbol{R}^{-1} \boldsymbol{r}(\boldsymbol{x}_{g}) + \sigma^{2} \boldsymbol{u}^{T}(\boldsymbol{x}_{g}) (\boldsymbol{F}^{T} \boldsymbol{R}^{-1} \boldsymbol{F})^{-1} \boldsymbol{u}(\boldsymbol{x}_{g})$$
(15)

where \mathbf{F} is the matrix of the basis function $\mathbf{f}(\mathbf{x}_g)$, i.e., $F_{ij} = B_j(\mathbf{x}_g^{(i)})$, i = 1, 2, ..., m; j = 1, 2, ..., p, $\mathbf{r}(\mathbf{x}_g)$ is the correlation between known a training points $\mathbf{x}_g^{(i)}$ and another point \mathbf{x}_g : $r_i = R(\mathbf{x}_g, \mathbf{x}_g^{(i)}, \boldsymbol{\theta})$, i = 1, 2, ..., m, \mathbf{R} is the autocorrelation matrix for known training points: $R_{ij} = R(\mathbf{x}_g^{(i)}, \mathbf{x}_g^{(j)}, \boldsymbol{\theta})$, i = 1, 2, ..., m; j = 1, 2, ..., m, and $u(\mathbf{x}_g) = \mathbf{F}^T \mathbf{R}^{-1} \mathbf{r}(\mathbf{x}_g) - \mathbf{f}(\mathbf{x}_g)$. Thus, $\hat{g}(\mathbf{x}_g)$ can be presented as follows:

$$\hat{g}(\mathbf{x}_g) \sim N\left(\mu_{\hat{g}}(\mathbf{x}_g), \sigma_{\hat{g}}^2(\mathbf{x}_g)\right)$$
 (16)

where $\mu_{\hat{g}}(x_g)$ is estimated Kriging mean and $\sigma_{\hat{g}}^2(x_g)$ is the corresponding variance, which is the uncertainty information. In adaptive Kriging methods for reliability analysis and RBDO, training points are adaptively added to refine the surrogate model until some criterion is met. The uncertainty information offered by the Kriging model can be used for the identification of next best training points in the population of MCS and to develop appropriate criteria to stop training. Many learning functions have been proposed to offer the instruction on training point selection and stopping criterion, such as U learning function (Echard et al., 2011) and expected feasibility function (EFF) (Bichon et al., 2012). Wang and Shafieezadeh (2018) proposed an efficient error rate-based stopping criterion (ESC) for adaptive reliability analysis. This stopping criterion will be used in this study. An overview of this approach is presented in the next sub-section.

3.2 Error-based stopping criterion for reliability analysis

The stopping criterion for ending the surrogate construction is quite important in adaptive Kriging methods. A loose stopping criterion may result in an inaccurate result, while an overly conservative one may lead to a large number of unnecessary trainings. To address this challenge, an efficient stopping criterion for reliability analysis named ESC was proposed in Wang and Shafieezadeh (2018). In ESC, the maximum error rate $\hat{\epsilon}_{max}$ for the estimated probability of failure is derived and taken as a criterion to evaluate the accuracy of the Kriging surrogate model in representing a performance function. This maximum error rate can be estimated using the following equation:

$$\hat{\epsilon}_{max} = max \left(\left| \frac{\widehat{N}_f}{\widehat{N}_f - \widehat{S}_f^u} - 1 \right|, \left| \frac{\widehat{N}_f}{\widehat{N}_f + \widehat{S}_s^u} - 1 \right| \right)$$
(17)

where \widehat{N}_f is the estimated number of failure points by the surrogate model, \widehat{S}_f^u and \widehat{S}_s^u are the upper bounds of \widehat{S}_f and \widehat{S}_s , respectively, \widehat{S}_f is the total number of wrong sign estimations in the estimated failure domain $\widehat{\Omega}_f$ by the surrogate model, and \widehat{S}_s is the one in estimated safe domain $\widehat{\Omega}_s$ by the surrogate model. It has been shown in Wang and Shafieezadeh (2018) that both \widehat{S}_s and \widehat{S}_f follow a Poisson binomial distribution with mean and variance shown below:

$$\hat{S}_{s} \sim PB \left(\sum_{i=1}^{\hat{N}_{s}} P_{i}^{wse}, \sum_{i=1}^{\hat{N}_{s}} P_{i}^{wse} \left(1 - P_{i}^{wse} \right) \right)$$

$$\chi_{i} \in \hat{\Omega}_{s}$$

$$(18)$$

$$\hat{S}_{f} \sim PB \left(\sum_{i=1}^{\hat{N}_{f}} P_{i}^{wse}, \sum_{i=1}^{\hat{N}_{f}} P_{i}^{wse} \left(1 - P_{i}^{wse} \right) \right)$$

$$x_{i} \in \hat{\Omega}_{f}$$

$$(19)$$

where PB represents the Poison Binomial distribution and P_i^{wse} is the probability of wrong sign estimation for x_i , which can be computed as $P_i^{wse} = \Phi\left(-\frac{|\mu_{\hat{g}}(x_g)|}{\sigma_{\hat{g}}(x_g)}\right)$, where $\Phi(\cdot)$ is the standard normal cumulative density function. Thus, the upper and lower bounds of \hat{S}_s and \hat{S}_f with a confidence level α can be found as:

$$\hat{S}_{s} \in \left(\boldsymbol{\theta}_{\hat{S}_{s}}^{-1}\left(\frac{\alpha}{2}\right), \boldsymbol{\theta}_{\hat{S}_{s}}^{-1}\left(1 - \frac{\alpha}{2}\right)\right) \tag{20}$$

$$\hat{S}_f \in \left(\boldsymbol{\theta}_{\hat{S}_f}^{-1} \left(\frac{\alpha}{2}\right), \boldsymbol{\theta}_{\hat{S}_f}^{-1} \left(1 - \frac{\alpha}{2}\right)\right) \tag{21}$$

where $\boldsymbol{\theta}_{\hat{S}_s}^{-1}$ and $\boldsymbol{\theta}_{\hat{S}_f}^{-1}$ are the inverse CDF of the Poisson binomial distribution. For the detail of the derivation, the reader is referred to Wang and Shafieezadeh (2018).

The estimate of the maximum error offers information on the accuracy of the constructed Kriging in terms of representing the reliability of the structure or system. For the adaptive process, a stopping criterion is set as $\hat{\epsilon}_{max} \leq \epsilon_{thr}$, where ϵ_{thr} is a prescribed threshold. The adaptive training process of the Kriging model can be terminated when $\hat{\epsilon}_{max}$ is smaller than the prescribed threshold ϵ_{thr} .

In existing RBDO methods that use adaptive surrogate models, the training points for different performance functions are often shared in the iterative process of the optimization, and the enrichment is performed for each surrogate model for the performance function in each iteration. This limitation is due to the fact that other than the convergence stopping criterion for the optimization process (e.g. the convergence check later described in Step 6 of Section 4.3), there is no stopping criterion for the surrogate models of individual performance functions. However due to different complexities of performance functions, the number of training points required for the surrogate model construction can be different. Therefore, some enrichment actions for some surrogate models, especially in the late period of the optimization process, can be unnecessary.

The ESC approach, albeit developed for reliability analysis, can be leveraged to avoid the unnecessary trainings of the surrogate model construction for RBDO, as reliability analysis is an essential part in RBDO. With the help of ESC, one can be notified of the accuracy of the current performance function surrogate models in terms of analyzing the reliability, and then can determine if additional surrogate model enrichment is still desired. Given such accuracy information, the training process of each surrogate model for the performance functions is allowed to be performed independently from each other. And in this fashion, unnecessary training for sufficiently accurate surrogate models can be avoided. In this study, a new quantile-based sequential RBDO method that takes advantage of the independent training is proposed in the next section.

4. The proposed quantile-based sequential method with error-controlled independent training and independent constraint boundary sampling

The main idea of the proposed method is similar to the one depicted in Fig. 4. Kriging surrogate models are used to replace the objective function and performance functions; however, ESC is integrated in a way that it allows independent training of the Kriging surrogate model for each performance function. The independent training allows all the training points of a surrogate model to be fully in favor of the construction for each individual performance function, hence providing

higher efficiency compared to traditional methods, which share training points among different performance function surrogate models. In addition, the independent training also facilitates a new sampling method based on CBS. While CBS considers only deterministic constraints and shares point among performance function surrogate models, the proposed sampling approach selects points considering the improvement of both deterministic and probabilistic constraints simultaneously for each surrogate model independently. The sampling of training points is first introduced in the next two sub-sections.

4.1 The training point sampling before optimization

Based on authors' experience, the initial training points can have a huge impact on the result. Insufficient number of initial training points may lead to a wrong final result; and too many training points unnecessarily add to the computational cost. To avoid both situations, an approach similar to the enrichment in Moustapha et al. (2016) is taken. Echard et al. (2011) proposed the *U* learning function, which is formulated as follows:

$$U = \frac{|\mu_{\hat{g}}(\mathbf{x}_g)|}{\sigma_{\hat{g}}(\mathbf{x}_g)} \tag{22}$$

When the value of the learning function is small for a point, it means either the limit state function value of the point is close to the limit state (i.e., the numerator is small), or we are uncertain about the limit state function value of the point (i.e., the denominator is large). The point with the smallest learning function value is of interest. This learning function is used as the sampling criterion and stopping criterion for reliability analysis as follows. The process adaptively adds the point with the smallest U from a MCS population until $\min_{x \in U}(U) > 2$. For the first step of Kriging construction

before the sequential process, only semi-accurate models are required. Thus, this criterion can be relaxed as follows:

$$\rho = \frac{n_{U>2}}{N_{mcs}} > \rho_{th} \tag{23}$$
 where $n_{U>2}$ is the number of points with a U learning function larger than 2, N_{mcs} is the total

where $n_{U>2}$ is the number of points with a *U* learning function larger than 2, N_{mcs} is the total population of MCS, thus, ρ is the percentage of points with a *U* learning function larger than 2 in the total population, and ρ_{th} is a prescribed threshold. In this study, it is found that 99% is a suitable value for ρ_{th} .

In the proposed method, for each performance function, LHS is first used to generate $(2n_d+1)$ points for the construction of the initial surrogate model. Then a sufficiently large MCS population is generated, and training points are adaptively added until $\rho > \rho_{th}$. Different from Li et al. (2019) and Li et al. (2020), the training of surrogate model for each performance function is independent of each other and doesn't share the training points. This allows the enrichment of the surrogate model to be specialized for each individual performance function and all training points for a surrogate model to help the construction exclusively, resulting in higher effectiveness. The aforementioned enrichment is only for the performance functions. For the objective function, $(2n_d+1)$ points via LHS are used for the initial construction of the surrogate model. Once the initial construction of the surrogate models for both objective and performance functions is complete, the method enters the sequential process described in Eq. (9) and (10) and a new adaptive enrichment approach is taken in the next step. This approach is introduced in the next sub-section.

4.2 A new sampling approach

During the process of sequential optimization, the adaptive enrichment of performance is continued. In each iteration of Eq. (9) and (10), new training points are added to refine the surrogate model. For the objective function, only the optimum in the feasible region is of interest, thus, the enrichment is focused on the current optimal point. In each iteration, the current optimal point is taken as the next training point for the surrogate model that represents the objective function.

For performance functions, according to Eq. (10), the offset is determined by $g_i\left(\mathbf{d}^{(k-1)}, \boldsymbol{\mu}_{x}^{(k-1)}, \boldsymbol{\mu}_{p}\right)$ and $CDF^{-1}(\Phi(\beta_i^t)|g_i)$. The former is the value of the performance function with respect to the previous optimal point. Naturally, same as the surrogate model construction for the objective function, the current optimal point should also be added as a training point. The latter is governed by the reliability of the structure or system with regard to the performance function, so the boundary between the safe domain Ω_s and failure domain Ω_f is important. Inspired by CBS (Lee and Jung, 2008), a new sampling approach is proposed here to facilitate the surrogate model construction.

The original CBS is defined as follows:

$$CBS = \begin{cases} \sum_{i=1}^{m} \phi(\frac{\mu_{\widehat{g_i}}(\mathbf{x}_g)}{\sigma_{\widehat{g_i}}(\mathbf{x}_g)}) & \text{if } \mu_{\widehat{g_i}}(\mathbf{x}_g) \ge 0 \,\forall i \\ 0 & \text{otherwise} \end{cases}$$
(24)

where ϕ is the standard normal probability density function (PDF). Similar to the U learning function, the CBS aims to locate the point that is close to the limit state and has large variance in the feasible domain. The value of CBS increases when the point approaches the vicinity of the boundary or has a large variance since PDF has the largest value when $\frac{\mu_{\widehat{g_l}}(x_g)}{\sigma_{\widehat{g_l}}(x_g)} = 0$; hence the name

constraint boundary sampling. In addition, the points in the infeasible domain are not of interest, so CBS becomes zero for infeasible points. However, in its original form, all constraints, i.e., performance functions, are considered simultaneously. And the training points are shared among performance functions. One problem is that the shared training points cannot be equally beneficial to all performance functions. In this study, thanks to the independent training, we propose a new sampling approach named independent constraint boundary sampling (ICBS) that is more effective for individual performance functions by virtue of independent training. The new ICBS is defined as follows:

$$ICBS_{1}^{i} = \begin{cases} \phi\left(\frac{\mu_{\widehat{g_{1}}}(\mathbf{x}_{g})}{\sigma_{\widehat{g_{1}}}(\mathbf{x}_{g})}\right) & \text{if } \mu_{\widehat{g_{1}}}(\mathbf{x}_{g}) \geq 0 \ \forall i \\ 0 & \text{otherwise} \end{cases}$$
where $ICBS_{1}^{i}$ is the sampling criterion for the i_{th} performance function. For the surrogate model of i_{th} performance function i_{th} and i_{th} performance i_{th} performance function i_{th} performance function.

where $ICBS_1^i$ is the sampling criterion for the i_{th} performance function. For the surrogate model of i_{th} performance function, the next "best" training point should be the point with the largest $ICBS_1^i$ value. As can be easily observed, this ICBS is just the original CBS that is focused on an individual performance function. When sampling the next best training point for a performance function, only the point that is close to boundary of this specific performance function and is also in the feasible region of this specific performance function is selected. This sampling approach can avoid the undesirable influence of other performance functions.

However, this *ICBS*₁ⁱ only considers deterministic constraints described in Eq. (1). As shown in Fig. 3, the optimal point is actually on active probabilistic constraint. The core of this quantile-based method is to transfer the RBDO problem into a serial of shifted deterministic optimization problems, of which the shifted deterministic constraints are equivalent to the probabilistic constraint. As a result, the accuracy of probabilistic constraints, i.e., shifted deterministic constraints, should also be guaranteed. In each iteration of adaptive Kriging method, not only is the "best" next training points for each deterministic constraint found, but also one for each probabilistic constraint is identified. The "best" point regarding the probabilistic constraints, similar to the deterministic constraints, is determined through the following equation:

$$ICBS_{2}^{i} = \begin{cases} \phi\left(\frac{\mu_{\widehat{g_{i}}}(\mathbf{x}_{g}) + c_{i}^{(k)}}{\sigma_{\widehat{g_{i}}}(\mathbf{x}_{g})}\right) & if \ \mu_{\widehat{g_{i}}}(\mathbf{x}_{g}) \ge 0 \ \forall i \\ 0 & otherwise \end{cases}$$
 (26)

Compared to $ICBS_1^i$, $ICBS_2^i$ aims to locate the point that is close to the probabilistic constraint boundary and has larger variance; the value of it increases when the point approaches the boundary of the probabilistic constraints or has a large variance, since PDF has the largest value when $\frac{\widehat{G_i}(x_g) + c_i^{(k)}}{\sigma_{\widehat{G}}(x_g)} = 0$. Similarly, the point with the largest value of $ICBS_2^i$ is the next best training point.

In our proposed method, for the surrogate model construction of an individual performance function, only one point is selected additional to the optimal point. Above all, considering both deterministic and probabilistic constraints, ICBS can be defined as follows:

$$ICBS^{i} = \begin{cases} max \left(\phi\left(\frac{\mu_{\widehat{g_{i}}}(\mathbf{x}_{g})}{\sigma_{\widehat{g_{i}}}(\mathbf{x}_{g})}\right), \phi\left(\frac{\mu_{\widehat{g_{i}}}(\mathbf{x}_{g}) + c_{i}^{(k)}}{\sigma_{\widehat{g_{i}}}(\mathbf{x}_{g})}\right) \right) & if \ \mu_{\widehat{g_{i}}}(\mathbf{x}_{g}) \ge 0 \ \forall i \end{cases}$$

$$otherwise$$

The point with the largest $ICBS^i$ should be the next training point. This $ICBS^i$ automatically chooses the "best" feasible point that benefits either the deterministic constraint or the probabilistic constraint the most based on the CBS values for both constraints. Note that in the original CBS, a sampling criterion considering the nearest distance from the existing training points to the sample point was also proposed. However, this sampling criterion requires the distance calculation for every training point candidate, hence the potential for high computational cost. To address this challenge, the skip scheme in Li et al. (2020) is adopted here: if the minimum distance from the next "best" point to the existing training points in the standard normal space is smaller than $0.2\beta_i^t$, the next "best" point is skipped. This scheme also helps the Kriging surrogate model avoid ill conditioning. In the next sub-section, the procedure of the proposed method is elaborated.

4.3 Procedure of the proposed method

With the help of ESC and independent training and ICBS, the main steps of the proposed method are summarized as follows:

- Step 1: Input the initial design point and initialize the offsets $c_i^{(0)}$. Input the initial design point: $[\mathbf{d}^{(0)}; \boldsymbol{\mu}_{x}^{(0)}]$. Meanwhile, initialize the offset for all performance functions: $c_i^{(0)} = 0$, i = 1, 2, ..., m.
- Step 2: Construct the surrogate models before sequential optimization. Use uniform distribution to generate $(2n_d + 1)$ LHS points for the objective function and each performance function. Then, for each performance function, generate an MCS population of the random variables with a size of 1×10^4 and from it adaptively add training points with the smallest U learning function value until the relaxed criterion described in Eq. (23) is met. The training point set for the objective function is denoted as S_0 ; and the training point set for the i_{th} performance function is denoted as S_i , i = 1, 2, ..., m.
- Step 3: Initialize the sequential optimization process. Set the iteration number k = 1, and set the training indicator $ind_i = 1, i = 1, 2, ..., m$ for all surrogate models of performance functions.
- Step 4: Sequential Optimization. Solve the deterministic optimization for the problem described in Eq. (9) and (10) using the offset $c_i^{(k-1)}$, i = 1, 2, ..., m and the current surrogate models for objective function and performance function. The current optimal result is $[d^{(k)}; \mu_x^{(k)}]$.
- Step 5: New offset calculation. Use $[\mathbf{d}^{(k)}; \boldsymbol{\mu}_{x}^{(k)}]$ as the mean and generate an MCS population S_c that is sufficient for the reliability analysis. For examples of this paper, the number is 1×10^6 . Fit a distribution to the MCS population using fittist in MATLAB and calculate the quantile corresponding to the target reliability probability: $CDF^{-1}(\Phi(\beta_i^t)|g_i)$. Then use Eq. (10) to calculate the new offset $c_i^{(k)}$.

- Step 6: Convergence check. Check if any of the convergence criteria is met: $\|c_i^{(k)} c_i^{(k-1)}\| \le 1.0 \times 10^{-3}$ or $\|[d^{(k)}; \mu_x^{(k)}] [d^{(k-1)}; \mu_x^{(k-1)}]\| \le 1.0 \times 10^{-3}$. If so, jump to Step 11. If not, go to Step 7.
- Step 7: Add the optimal point as the training point for the objective function. For the objective function surrogate model, if the minimum distance from the current optimal point to the points in S_0 in the standard normal space is larger than $0.2 \min (\beta_i^t)$, i = 1, 2, ..., m, add the optimal point as the training point; otherwise, skip the optimal point.
- Step 8: Training indicator update. If the distance between $[\boldsymbol{d}^{(k)}; \boldsymbol{\mu}_{x}^{(k)}]$ and $[\boldsymbol{d}^{(k-1)}; \boldsymbol{\mu}_{x}^{(k-1)}]$ in the standard normal space is larger than 0.2 $min(\beta_{i}^{t})$, i=1,2,...,m, set $ind_{i}=1,i=1,2,...,m$.
- Step 9: Ignore the inactive constraints' training. As the optimization proceeds, the training of surrogate models for the inactive constraints is not necessary. However, in the first few iterations, the determination of activity of constraints may not be accurate. Therefore, after a few iterations (5 is used in the paper, however, a large number can be used to ensure the accuracy in practice), we can ignore the inactive constraints. When k > 5, set $ind_i = 0$ for the inactive constraints in the result of Step 4.
- Step 10: Add training points for performance functions. For the i_{th} performance function surrogate model with $ind_i = 1$, if the minimum distance from the current optimal point to the points in S_i in the standard normal space is larger than $0.2\beta_i^t$, add the optimal point to S_i ; otherwise, skip the optimal point. In addition, for the i_{th} performance function surrogate model with $ind_i = 1$, select the "best" point based on ICBS using Eq. (27), if the minimum distance from the "best" point to the points in S_i in the standard normal space is larger than $0.2\beta_i^t$, add the "best" point to S_i ; otherwise, skip the optimal point.
- Step 11: Error-based stopping criterion check. For the i_{th} performance function surrogate model with $ind_i = 1$, use Eq. (21) to calculate the maximum error of the surrogate model in terms of failure probability, if the maximum error is smaller than the prescribed threshold ϵ_{thr} , set $ind_i = 0$; otherwise, set $ind_i = 1$.
- Step 12: Update the surrogate models. Use the updated S_0 and S_i , i = 1, 2, ..., m, to construct the new surrogate models for the objective function and performance functions, respectively. k = k + 1. Then, jump back to Step 4.
- Step 13: End. The result is final and end the process.

The flowchart of the proposed method is presented in Fig. 5-6. Fig. 6 is a supplement to Fig. 5. In the proposed method, the error-based stopping criterion allows the understanding of the accuracy of an individual performance function with regards to the reliability. When the surrogate model of a performance function is sufficiently accurate, i.e., $\hat{\epsilon}_{max} \leq \epsilon_{thr}$, adding new training points is not necessary. By avoiding unnecessary function evaluations, the computational cost is reduced. Note that when the current optimal point moves to a certain degree from the previous point (it is defined in Step 8 as the distance between $[\boldsymbol{d}^{(k)};\boldsymbol{\mu}_x^{(k)}]$ and $[\boldsymbol{d}^{(k-1)};\boldsymbol{\mu}_x^{(k-1)}]$ in the standard normal space being larger than 0.2 min (β_i^t) , i = 1, 2, ..., m), the previous maximum errors may not be representative anymore, thus, new training points are still required and the maximum error needs to be reevaluated in the iteration. In addition, in Step 9, the inactive constraints, which are not our main focus, are ignored for adding training points to further avoid unnecessary function evaluations. Ignoring the inactive constraints can be crucial as for inactive constraints the actual failure probabilities are often extremely small, resulting in difficulties in the refinement of the surrogate model. Without ignoring the inactive constraints, significantly more training points needed to satisfy the ESC requirement. The points that are too close to the existing training points are also skipped as in Step 7 and 10. The proposed ICBS helps to refine the surrogate models considering both deterministic and probabilistic constraints. The performance of the proposed method is demonstrated through five numerical examples in the next section.

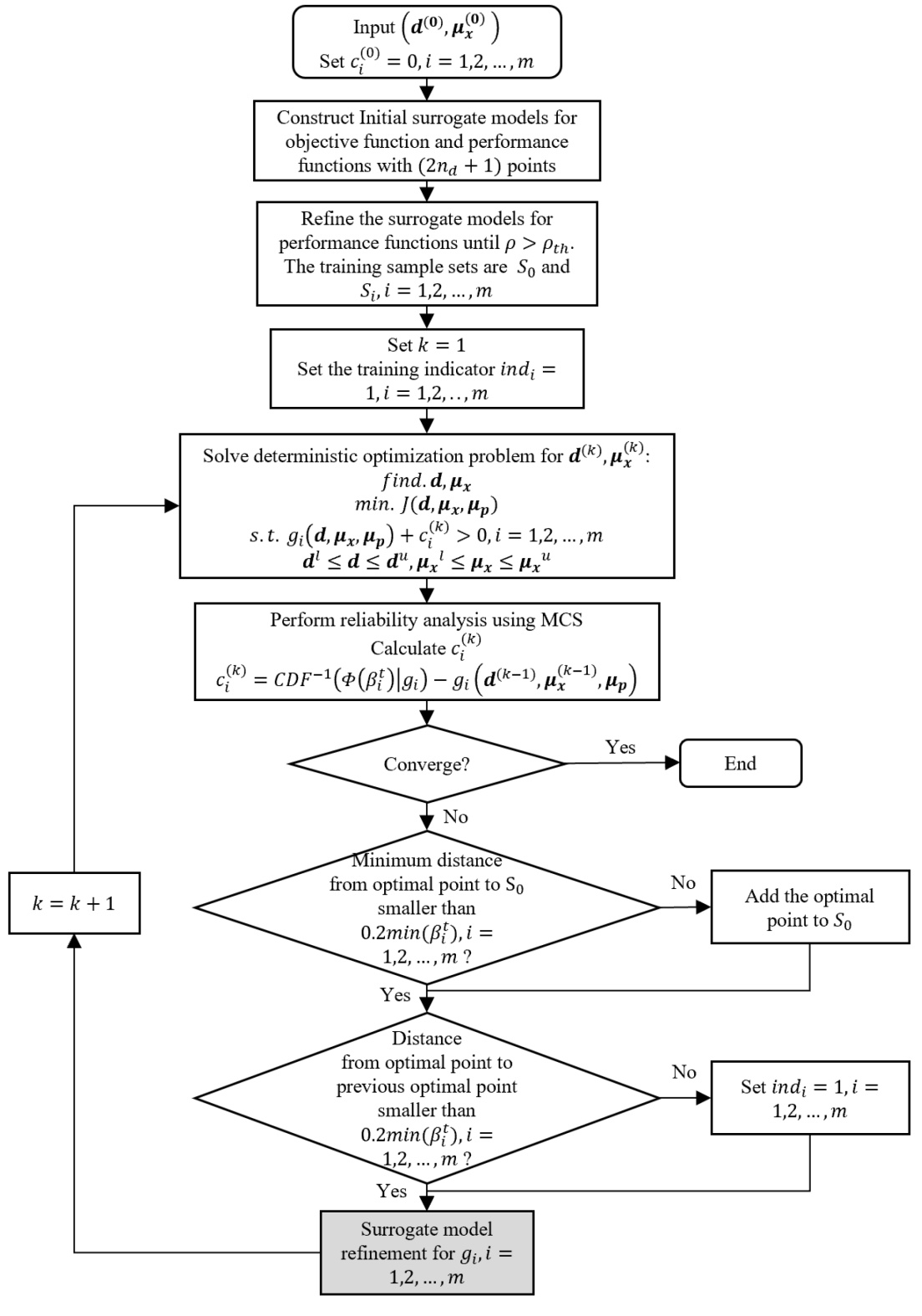


Fig. 5 Flowchart of the proposed method: Part A

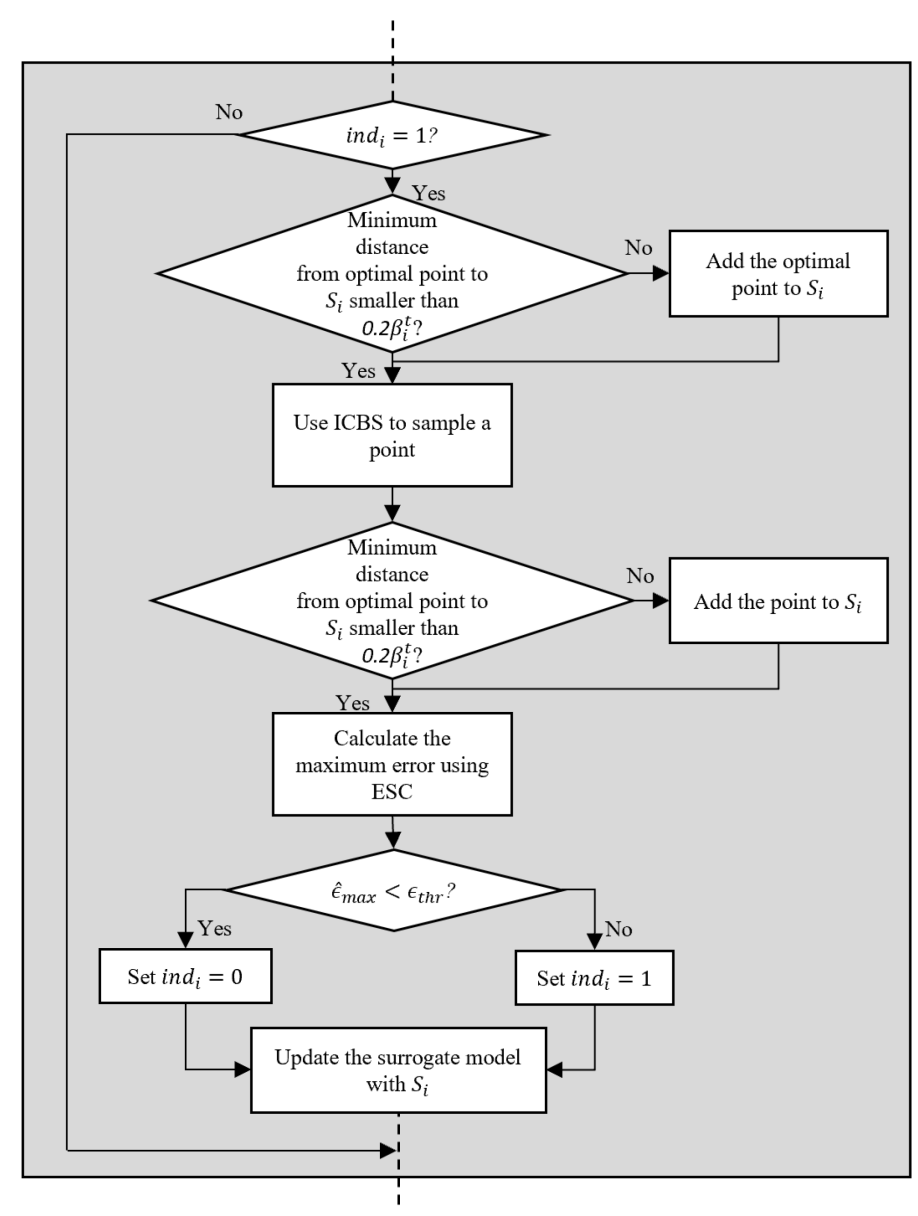


Fig. 6 Flowchart of the proposed method: Part B. Surrogate model refinement for each g_i

5. Numerical Examples

In this section, the performance of the proposed method along with several state-of-the-art methods are compared for four representative mathematical and engineering examples and one application example on the optimization of overhead transmission line. The prescribed threshold ϵ_{thr} is set to 5% and ρ is set to 99%. The function call comparisons for all examples are based on the assumption that the constraint functions are independent from each other. All numerical examples are tested using the DACE toolbox (Lophaven et al., 2002a, 2002b) in MATLAB 2019a.

5.1 Classic 2D problem

The first numerical example is a classical 2D RBDO problem that has been widely used in the literature (Cho and Lee, 2011; Li et al., 2019; Yang and Gu, 2004; Yi et al., 2016). It has two random design variables and three nonlinear constraints. The two random design variables are

statistically independent and follow normal distributions. The center point $[5, 5]^T$ is selected as the initial design point. The problem is formulated as follows:

$$find. \boldsymbol{\mu}_{x} = [\mu_{x1}, \mu_{x2}]^{T}$$

$$min. \ \mu_{x1} + \mu_{x2}$$

$$s.t. \begin{cases} Pr(g_{i}(\boldsymbol{x}) > 0) \leq \Phi(-\beta_{i}^{t}), \ \beta_{i}^{t} = 3, \ i = 1,2,3 \end{cases}$$

$$0 \leq \mu_{x1} \leq 10, \ 0 \leq \mu_{x2} \leq 10$$

$$x_{j} \sim N(\mu_{xj}, 0.3^{2}), \ j = 1,2$$

$$(28)$$

where

$$g_{1}(\mathbf{x}) = 1 - \frac{x_{1}^{2}x_{2}}{20},$$

$$g_{2}(\mathbf{x}) = 1 - \frac{(x_{1} + x_{2} - 5)^{2}}{30} - \frac{(x_{1} - x_{2} - 12)^{2}}{120},$$

$$g_{3}(\mathbf{x}) = 1 - \frac{80}{x_{1}^{2} + 8x_{2} + 5}$$
The constraint comparison for the surrogate models and the true performance of the surrogate models.

Fig. 7 shows the constraint comparison for the surrogate models and the true performance functions along with the training points before and in the optimization process. As shown in the figures, the training points are characterized for each performance function independently. In this manner, the surrogate models can be built more efficiently. It can also be observed that the surrogate models are quite accurate in the region of active constraints, while $\hat{g}_3(x)$ is not quite accurate. However, $\hat{g}_3(x)$ is not an active constraint, so it is not of much interest. The trends of maximum error estimated using ESC for the two active constraints are shown in Fig. 8. The maximum errors for $\hat{g}_1(x)$ and $\hat{g}_2(x)$ reach the threshold at fourth and eighth generation, respectively, indicating both surrogate models are sufficiently accurate to represent the reliability of the system. For the objective function, the training point number are 9, and for the three performance functions, the numbers are 13, 10 and 14, respectively. The final results of the proposed method are shown in Table 1. Compared with other RBDO methods (SLSV and SORA (Yang and Gu, 2004); ASORA (Yi et al., 2016); SSRBO (Li et al., 2019)), it can be observed that the proposed method substantially reduces the number of function evaluations. In this example, the strategy of ignoring inactive constraints does have a significant impact, as during the process the distance that the estimated optimal point moves exceeds the criterion of 0.2 min (β_i^t) defined in Step 8, resulting in the reactivation of the refinement of the inactive constraint surrogate model. However, with the help of ICBS, the efficiency of the refinement of surrogate models are improved compared to all the other methods, as for each active constraint surrogate model the number of training points has been significantly reduced. Due to the stochasticity in the construction of the Kriging model, which results from randomness in the initial training points, the computation using the proposed method is repeated ten times to test the robustness. The number of function evaluations fluctuates between 43 and 59, which are all far smaller than the existing methods.

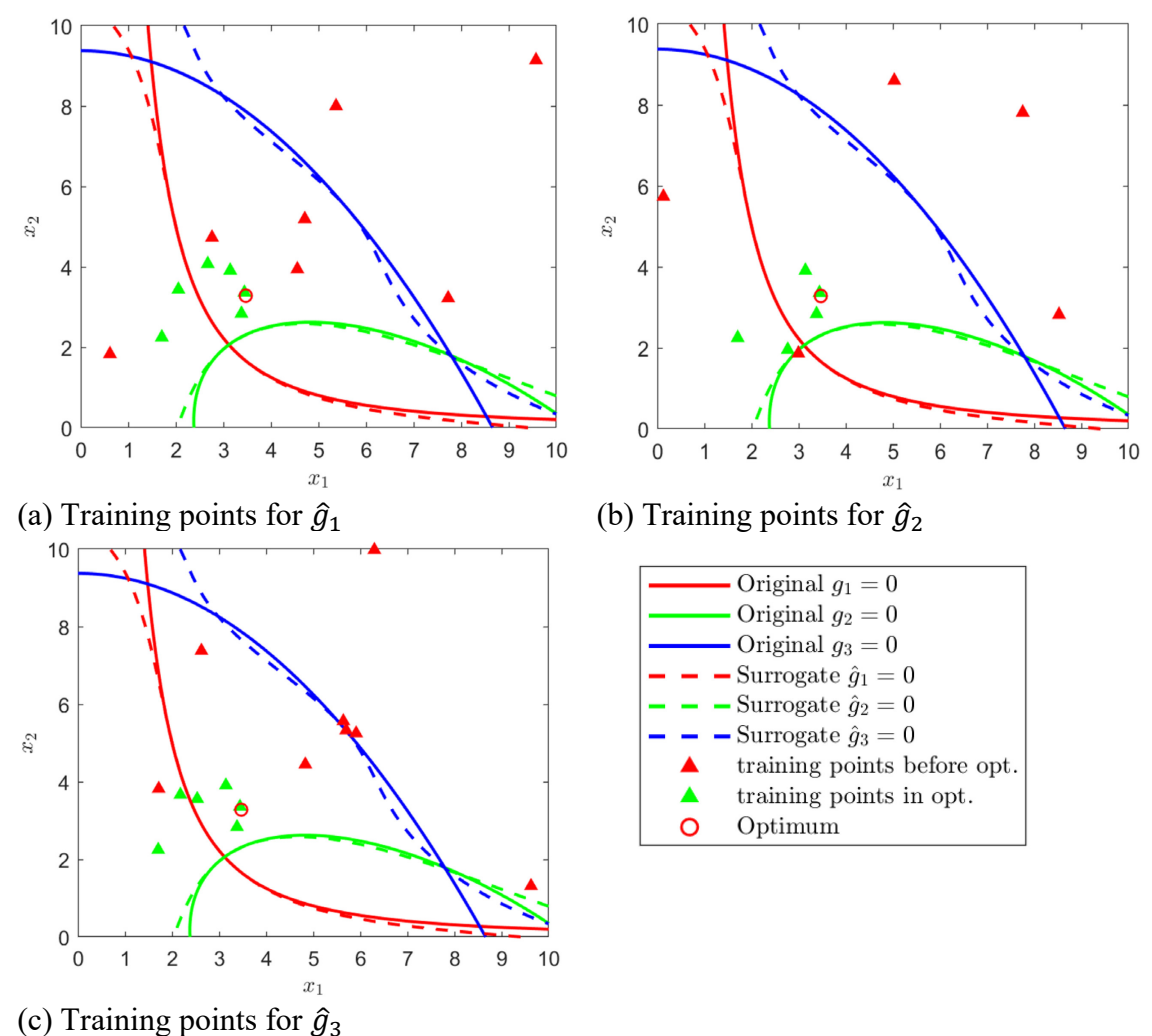


Fig. 7 Constraint comparison and training points for Example 1

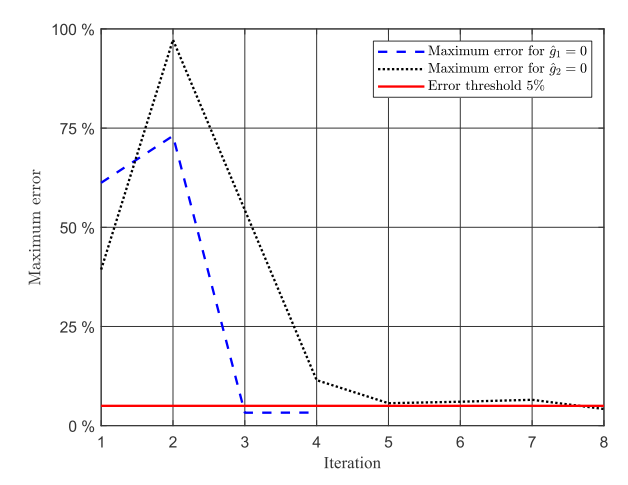


Fig. 8 Maximum error trends for the two active constraints

Table 1 Final result and comparison with other methods for Example 1

Method	Optimum	$oldsymbol{eta}_1$	$oldsymbol{eta}_2$	$N_{total}(N_{obj} + N_{con})$
SLSV	6.731 (3.434, 3.297)	2.97	3.09	539(55+484
SORA	6.743 (3.458, 3.285)	2.97	3.05	510(55+455)
ASORA	6.743 (3.458, 3.285)	2.97	3.05	68(20+48)
SSRBO	6.743 (3.458, 3.285)	3.009	3.012	$112(28+28\times3)$
Proposed	6.751 (3.467, 3.282)	3.054	3.017	46(9+37)

5.2 Highly nonlinear 2D problem with multiple MPPs

The second problem is the modified Haupt example in Li et al. (2020). It has two random design variables and two constraints. One constraint concerns a highly nonlinear function and has multiple MPPs, and the other constraint is a linear function. The two random design variables are statistically independent and follow normal distributions. The initial design point is [2:83 3.52]^T, which is the same as Li et al. (2020). The problem is formulated as follows:

find.
$$\mu_{x} = [\mu_{x1}, \mu_{x2}]^{T}$$

min. $(\mu_{x1} - 2.9)^{2} + (\mu_{x2} - 3.7)^{2}$
 $s.t.\begin{cases} Pr(g_{i}(\mathbf{x}) > 0) \leq \Phi(-\beta_{i}^{t}), & \beta_{i}^{t} = 2, & i = 1,2 \\ 0 \leq \mu_{x1} \leq 3.7, & 0 \leq \mu_{x2} \leq 4 \\ x_{j} \sim N(\mu_{xj}, 0.2^{2}), & j = 1,2 \end{cases}$
(30)

where

$$g_1(x) = x_1 \sin(4x_1) + 1.1 \sin(2x_2),$$

$$g_2(x) = 3 - x_1 - x_2$$
(31)

Fig. 9 shows the constraint comparison for the surrogate models and the true performance functions along with the training points before and in the optimization process. The linear constraint $\hat{g}_2(x)$ is simple and inactive, so it is not of interest. The training points are shown for $\hat{g}_1(x)$. It can be observed that near the active constraint, the surrogate model $\hat{g}_1(x)$ is quite accurate. Before the optimization process, training points are focused on the deterministic constraint; however, in the optimization process, most training points are selected near the probabilistic constraint. For the objective function, the training point number are 10, and for the two performance functions, the numbers are 20 and 9, respectively. With only 39 function evaluations, the proposed method is able to converge to the final result. Although the reliability is 1.988, which is slightly smaller than the target reliability of 2, the error of the failure probability compared with the actual one is 2.6%, which is smaller than the maximum error estimated by the ESC: 4.3% and within the error threshold 5%, indicating the effectiveness of ESC in the proposed method. The final results of the proposed method are compared with other RBDO methods (PMA and Li et al. (2020)). It can be observed that the function evaluations are significantly fewer than other methods. In this example, the strategy of ignoring inactive constraints takes effects and ends the refinement of $\hat{g}_2(x)$ early, thus, avoiding unnecessary training. For the active constraint surrogate model, $\hat{g}_1(x)$, the number of training points has been reduced from 29 to 20, as the ICBS helps to locate the most suitable training points without being affected by the information from $\hat{g}_2(x)$. For this numerical example, the computation is also repeated ten times to test the robustness. It is observed that the number of function evaluations fluctuates between 37 and 54, which are all far smaller than the existing methods.

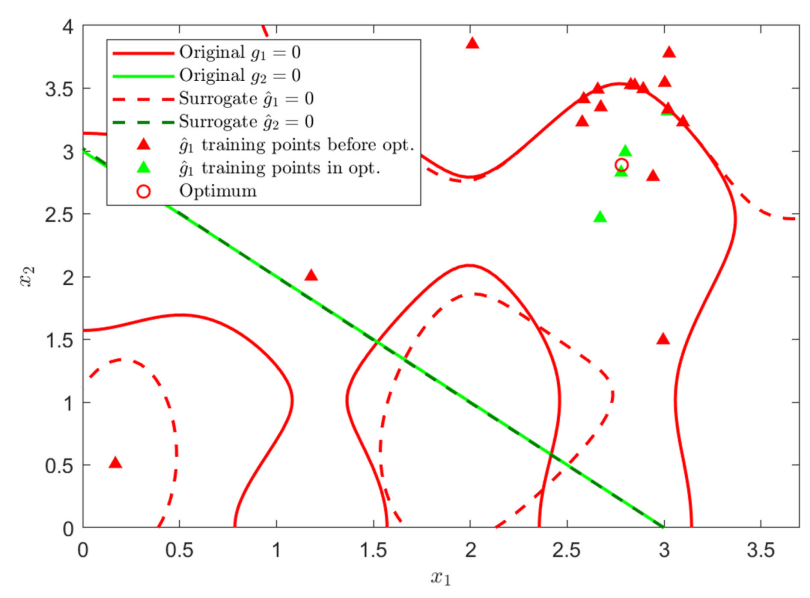


Fig. 9 Constraint comparison and training points for Example 2

Table 2 Final result and comparison with other methods for Example 2

Method	Optimum	$oldsymbol{eta_1}$	$N_{total}(N_{obj} + N_{con})$
PMA(HMV)	0.4772 (2.772, 3.021)	1.593	1286
Li et al. (2020)	0.6828 (2.790, 2.879)	1.999	78 (26+26×2)
Proposed	0.6716 (2.783, 2.889)	1.988	39 (10+29)

5.3 Welded beam problem

The welded beam problem (Lee and Lee, 2005; Ramakrishnan and Rao, 1996; Song et al., 2019; Yi et al., 2016) aims to minimize the welding cost when subject to constraints on geometry, maximum possible stress, and tip deflection. The welded beam structure is shown in Fig. 10. The four random design variables are depth and length of welding and height and thickness of the beam, and they are statistically independent and follow normal distributions. The initial design point is taken as [6.207, 157.8, 210.6, 6.207]^T, which is the solution to the deterministic optimization. The problem can be formulated as follows:

$$find. \boldsymbol{\mu}_{x} = [\mu_{x1}, \mu_{x2}, \mu_{x3}, \mu_{x4}]^{T}$$

$$min. \ c_{1}\mu_{x1}^{2}\mu_{x2} + c_{2}\mu_{x3}\mu_{x4}(z_{2} + \mu_{x2})$$

$$s.t.\begin{cases} Pr(g_{i}(x) > 0) \leq \Phi(-\beta_{i}^{t}), \ \beta_{i}^{t} = 3, \ i = 1,2,...,5 \end{cases}$$

$$s.t.\begin{cases} 3.175 \leq \mu_{x1} \leq 10, \ 150 \leq \mu_{x2} \leq 254, \ 200 \leq \mu_{x3} \leq 220, \ 3.175 \leq \mu_{x4} \leq 10 \end{cases}$$

$$x_{1} \sim N(\mu_{x1}, 0.1693^{2}), \ x_{2} \sim N(\mu_{x2}, 0.1693^{2}), \ x_{3} \sim N(\mu_{x3}, 0.0107^{2}), \ x_{4} \sim N(\mu_{x4}, 0.0107^{2}) \end{cases}$$

$$(32)$$

where

$$g_{1}(\mathbf{x}) = \frac{\tau(\mathbf{x})}{z_{6}} - 1, \quad g_{2}(\mathbf{x}) = \frac{\sigma(\mathbf{x})}{z_{7}} - 1,$$

$$g_{3}(\mathbf{x}) = \frac{x_{1}}{x_{4}} - 1, \quad g_{4}(\mathbf{x}) = \frac{\delta(\mathbf{x})}{z_{5}} - 1, \quad g_{5}(\mathbf{x}) = 1 - \frac{P_{c}(\mathbf{x})}{z_{1}},$$

$$\tau(\mathbf{x}) = \left\{ t(\mathbf{x})^{2} + 2t(\mathbf{x})tt(\mathbf{x}) \frac{x_{2}}{2R(\mathbf{x})} + tt(\mathbf{x})^{2} \right\}^{1/2},$$

$$t(\mathbf{x}) = \frac{z_{1}}{\sqrt{2}x_{1}x_{2}}, \quad tt(\mathbf{x}) = M(\mathbf{x}) \frac{R(\mathbf{x})}{K(\mathbf{x})},$$
(33)

$$M(\mathbf{x}) = z_1 \left(z_2 + \frac{x_2}{2} \right), \quad R(\mathbf{x}) = \frac{\sqrt{x_2^2 + (x_1 + x_3)^2}}{2},$$

$$K(\mathbf{x}) = \sqrt{2}x_1x_2 \left\{ \frac{x_2^2}{12} + \frac{(x_1 + x_3)^2}{2} \right\}, \quad \sigma(\mathbf{x}) = \frac{6z_1z_2}{x_3^2x_4},$$

$$\delta(\mathbf{x}) = \frac{4z_1z_2^3}{z_3x_3^2x_4}, P_c(\mathbf{x}) = \frac{4.013x_3x_3^3\sqrt{z_3z_4}}{6z_2^2} \left(1 - \frac{x_3}{4z_2} \sqrt{\frac{z_3}{z_4}} \right),$$

where parameters can be found in Table 3.

 Table 3 Welded beam parameters

$\overline{z_1}$	$2.6688 \times 10^4 (N)$	Z ₆	9 . 377 ×10 (MPa)
z_2	$3.556 \times 10^2 (mm)$	z_7	$2.0685 \times 10^{2} (MPa)$
z_3	$2.0685 \times 10^{5} (MPa)$	c_1	$6.74135 \times 10^{-5} (\text{\$/mm}^3)$
z_4	$8.274 \times 10^4 (MPa)$	c_2	$2.93585 \times 10^{-6} (\$/\text{mm}^3)$
z_5	6.35 (mm)		

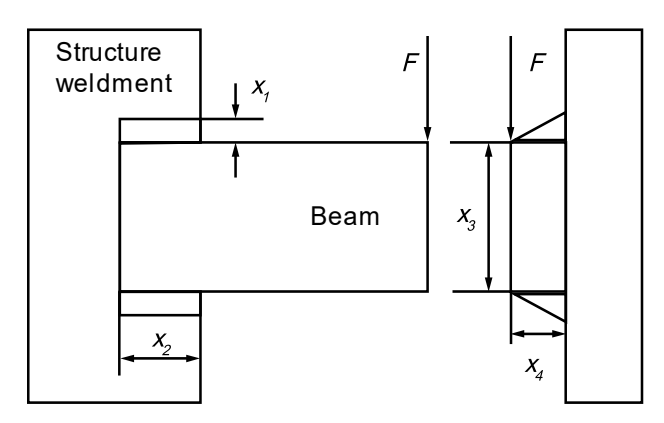


Fig. 10 Welded beam structure

For the objective function and three performance functions, the training point number are 15, 24, 22, 18, 20 and 21, respectively. The final results of the proposed method are shown in Table 4. The results are also compared with other RBDO methods (SORA and ASORA (Yi et al., 2016); SORA-ICDE (Ho-Huu et al., 2016); Song et al. (2019)). The reliability of the active constraints is calculated using MCS, and the number of function evaluations are the sum of objective and constraint function evaluation. The function evaluations needed by the proposed method are significantly fewer than other existing RBDO methods. In this example, the effect of ICBS is demonstrated by the fact that the active constraint surrogate model that uses the most training points, $\hat{g}_1(x)$, only uses 23 training points for the refinement, while the other Kriging-based method uses 46 training points for each constraint surrogate model. The computation is repeated ten times to test the robustness, the number of function evaluations fluctuates between 101 and 129, which are all far smaller than the existing methods.

Table 4 Final result and comparison with other methods for Example 3

Method	Optimum	$oldsymbol{eta_1}$	$oldsymbol{eta}_2$	β_3	$oldsymbol{eta}_5$	$N_{total}(N_{obj} + N_{con})$
SORA	2.592 (5.731, 200.93, 210.64, 6.242)	3.01	3.58	3.01	2.98	198(125+73)
ASORA	2.592 (5.731, 200.93, 210.64, 6.242)	3.01	3.58	3.01	2.98	167(77+90)
SORA-ICDE	2.593 (5.730, 201.00, 210.63, 6.240)	3.01	3.29	3	3.12	2119
Song et al. (2019)	2.591 (5.729, 200.90, 210.60, 6.239)	3.01	3.29	3	3.12	275(45+46×5)

5.4 Speed reducer problem

The fourth example is the well-known speed reducer problem that is used in the literature (Lee and Lee, 2005; Li et al., 2020, 2019; Rao, 2019; Song et al., 2019). The objective is to minimize the weight of a speed reducer, and the eleven constraints are set on bending and contact stress, longitudinal displacement, stress of the shaft, and geometry. The schematic speed reducer configuration is shown in Fig. 11. The seven random design variables are gear width, teeth module, number of teeth in the pinion, distance between bearings, and axis diameter. These variables are statistically independent and follow normal distributions. The initial design point is taken as [3.5, 0.7, 17, 7.3, 7.72, 3.35, 5.29]^T, which is the same as Li et al. (2020). The problem can be formulated as follows:

find:
$$\mu_{\mathbf{x}} = [\mu_{x1}, \mu_{x2}, \mu_{x3}, \mu_{x4}, \mu_{x5}, \mu_{x6}, \mu_{x7}]^{T}$$

min. $0.7854x_{1}x_{2}^{2}(3.3333x_{3}^{3} + 14.9334x_{3} - 43.0934) - 1.508x_{1}(x_{6}^{2} + x_{7}^{2})$
 $+7.477(x_{6}^{3} + x_{7}^{3}) + 0.7854(x_{4}x_{6}^{2} + x_{5}x_{7}^{2})$
 $\begin{cases} Pr(g_{i}(\mathbf{x}) > 0) \leq \Phi(-\beta_{i}^{t}), & \beta_{i}^{t} = 3, & i = 1,2,...,11 \\ 2.6 \leq \mu_{x1} \leq 3.6, & 0.7 \leq \mu_{x2} \leq 0.8, & 17 \leq \mu_{x3} \leq 28, \\ 7.3 \leq \mu_{x4} \leq 8.3, & 7.3 \leq \mu_{x5} \leq 8.3, & 2.9 \leq \mu_{x6} \leq 3.9, \\ 5.0 \leq \mu_{x7} \leq 5.5 \\ x_{i} \sim N(\mu_{xi}, 0.005^{2}) \end{cases}$
(34)

where

$$g_{1}(\mathbf{x}) = \frac{27}{x_{1}x_{2}^{2}x_{3}} - 1, \quad g_{2}(\mathbf{x}) = \frac{397.5}{x_{1}x_{2}^{2}x_{3}^{2}} - 1, \quad g_{3}(\mathbf{x}) = \frac{1.93x_{4}^{3}}{x_{2}x_{3}x_{6}^{4}} - 1,$$

$$g_{4}(\mathbf{x}) = \frac{1.93x_{5}^{3}}{x_{2}x_{3}x_{7}^{4}} - 1, \quad g_{5}(\mathbf{x}) = \frac{\sqrt{(745x_{4}/(x_{2}x_{3}))^{2} + 16.9 \times 10^{6}}}{0.1x_{6}^{3}} - 1100,$$

$$g_{6}(\mathbf{x}) = \frac{\sqrt{(745x_{5}/(x_{2}x_{3}))^{2} + 157.5 \times 10^{6}}}{0.1x_{6}^{3}} - 850, \quad g_{7}(\mathbf{x}) = x_{2}x_{3} - 40,$$

$$g_{8}(\mathbf{x}) = 5 - \frac{x_{1}}{x_{2}}, \quad g_{9}(\mathbf{x}) = \frac{x_{1}}{x_{2}} - 12, \quad g_{10}(\mathbf{x}) = \frac{1.5x_{6} + 1.9}{x_{4}} - 1,$$

$$g_{11}(\mathbf{x}) = \frac{1.1x_{7} + 1.9}{x_{5}} - 1$$
(35)

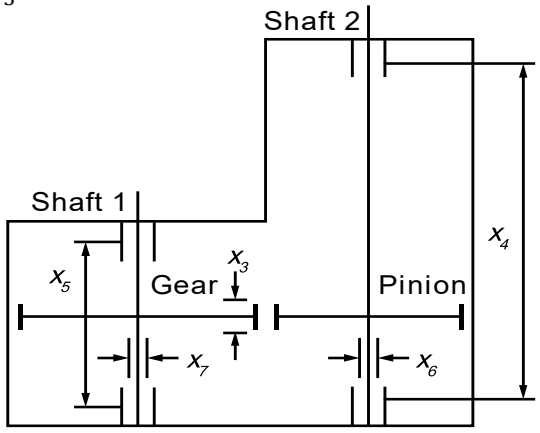


Fig. 11 Speed reducer structure

For the objective function and three performance functions, the training point number are 15, 24, 22, 18, 20 and 21, respectively. The comparison of the results yielded by the proposed method

and other state-of-the-art methods (SORA and ASORA (Yi et al., 2016); SSRBO (Li et al., 2019); Li et al. (2020); Song et al. (2019)) are presented in Table 5. The reliability of the active constraints is calculated using MCS, and the number of function evaluations are the sum of objective and constraint function evaluations. The proposed method is able to converge to optimal result with only 269 function evaluations in total, while other methods need more than 400 function evaluations. In this example, the effect of ICBS is demonstrated by the fact that the active constraint surrogate model that uses the most training points, $\hat{g}_5(x)$, only uses 29 training points for the refinement, while all the other Kriging-based methods use around 40 training points for each constraint surrogate model. For the speed reducer problem, the computation is also repeated ten times to test the robustness of the proposed approach. It is observed that the number of function evaluations fluctuates between 259 and 292, which are all far smaller than the existing methods.

Table 5 Final result and comparison with other methods for Example 4

Method	Optimum	$oldsymbol{eta}_5$	$oldsymbol{eta}_6$	$oldsymbol{eta}_8$	β_{11}	$N_{total}(N_{obj} + N_{con})$
SORA	3040.02 (3.580, 0.7, 17, 7.3, 7.764, 3.366, 5.301)	3.15	3.08	3.07	4.21	521(21+500)
ASORA	3038.61 (3.577, 0.7, 17, 7.3, 7.754, 3.365, 5.301)	3.18	3.08	3.07	4.21	418(22+396)
SSRBO	3038.66 (3.577, 0.7, 17, 7.3, 7.754, 3.366, 5.301)	3.13	2.95	3.01	3.09	468(39+39×11)
Li et al (2020)	3038.61 (3.577, 0.7, 17, 7.3, 7.754, 3.365, 5.302)	2.998	2.989	3.00	3.00	$492(41+41\times11)$
Song et al. (2019)	3038.61 (3.577, 0.7, 17, 7.3, 7.754, 3.365, 5.302)	3.00	3.01	3.01	3.00	$422(37+35\times11)$
Proposed	3038.98 (3.577, 0.7, 17, 7.3, 7.754, 3.365, 5.302)	3.004	3.020	3.016	3.009	269 (21+248)

5.5 Overhead transmission line problem

The last example is on the optimization of an overhead transmission line, which demonstrates a practical application of the proposed method to a problem with independent limit state functions. The objective of this example is to optimize the costs of the transmission tower and conductors under the constraints that both the tower and conductors satisfy their performance requirements considering uncertainties. Note that the analyses of the conductors and the towers are performed independently as they can be dynamically decoupled due to the large differences in their dynamic characteristics (e.g., dominant modal frequencies) and the computational cost of analyzing conductors and tower simultaneously in one computational environment is very high. As a result, past studies have decoupled towers and conductors and investigated their performance using independent models (Darestani et al., 2020; Ma et al., 2020). As a result, an independent surrogate model can be constructed for each model. In studies focused on the analysis of the transmission line systems, the conductors and the tower can both have high-fidelity finite element models. The models of the conductors and the transmission tower are simplified herein, and some assumptions are made. As the example is for the purpose of demonstration, further studies with realistic finite element models and wind models can be pursued in future research.

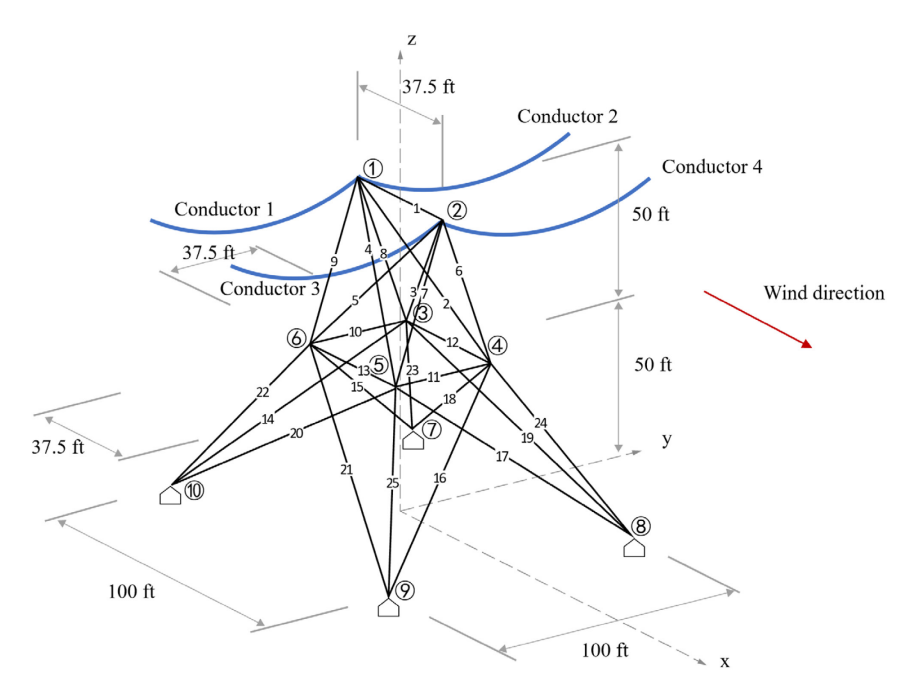


Fig. 12 Tower and conductors

The tower considered here is a 25-member space truss as shown in Fig. 12. Similar structures are investigated in many other studies (Ho-Huu et al., 2016; Saka, 1990; Toğan and Daloğlu, 2008). The structure herein is scaled up to a size of an actual transmission tower (100 ft) as shown in the figure. Members of the tower are categorized into 6 groups, which are denoted as $[A_1, A_2, ..., A_6]^T$ (unit: in²), and each of them is regarded as a random design variable that follows a lognormal distribution. The grouping details are shown in Table 6. Four conductors are attached to the top two nodes of the truss as shown in Fig. 12. All conductors are considered as 1410 ft long on a 1400 ft span as shown in Fig. The conductors and the tower are both subject to wind loads that are in the x direction as shown in the figure, and the weight on the conductors are also considered. The diameter of the conductor CD is considered as a random design variable that follows a lognormal distribution. The random parameters considered herein are the modulus of elasticity of the tower E and the 3-second gust wind velocity at 10 m above the ground line V (unit: mph), which follow a lognormal distribution and a Gumbel distribution, respectively. All the random design variables are stored in the vector $[A_1, A_2, ..., A_6, CD]^T$, and all the random parameters are stored in the vector $[E, V]^T$. The limit state for the tower is a displacement of 20 inch on either Node 1 or 2; and the limit state for the conductor is the tensile strength of 32,000 psi.

Table 6 Grouping details for Example 5

Group	Member No.
A_1	1,10,11
A_2	2,3,4,5
A_3^-	6,7,8,9,22,23,24,25
A_4	12,13
A_5	14,15,16,17
A_6	18,19,20,21

Wind loads depend on multiple factors. According to ASCE 7-10 (2016) the wind load per unit length for a non-building structure can be determined using the following formula:

$$f_w = q_z G C_f D \tag{36}$$

where q_z is the velocity pressure at height z on the tower, G is the gust-effect factor (taken as 0.85), C_f is the force coefficient, and D is the diameter perpendicular to the wind direction (unit: ft). The force coefficient C_f considered herein is 2. Alternatively, the wind load on a non-structure building can be determined using the following formula:

$$F_w = q_z G C_f A_f \tag{37}$$

where A_f is projected area perpendicular to the wind direction. The wind velocity pressure is calculated as follows:

$$q_z = 0.613K_z K_d K_{zt} K_e V^2 (38)$$

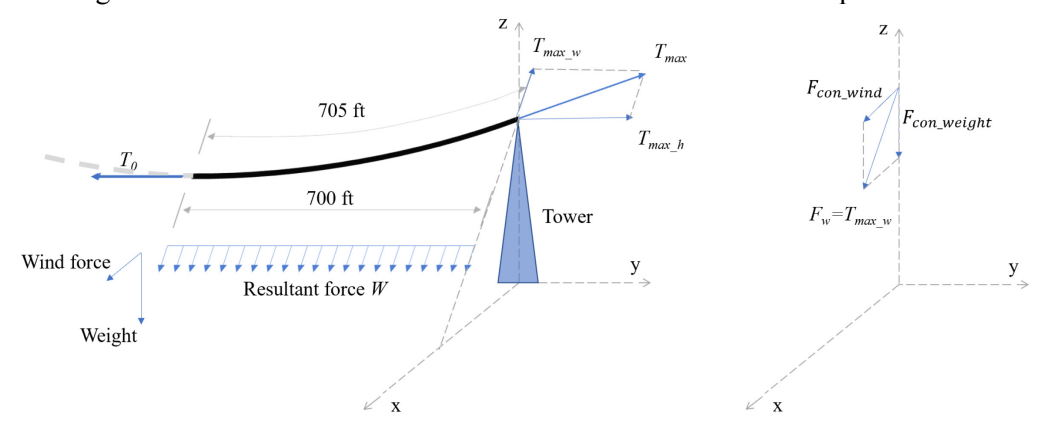
 $q_z = 0.613 K_z K_d K_{zt} K_e V^2$ (38) where K_z is the velocity pressure exposure coefficient, K_d is the wind directionality factor (taken as 1), K_{zt} is the wind topographic factor (taken as 1), K_e is the elevation factor (taken as 1). The velocity pressure exposure coefficient K_z can be calculated using the following formula:

$$K_z = 2.01 \left(\frac{\max{(15, z)}}{z_g}\right)^{2/\alpha}$$
 (39)

where z is the height from the ground line, and α and z_g are 9.5 and 900 ft, respectively. The conductor is considered to be at the height of 100 ft, thus, using Eq. (36), (38) and (39) the wind load per unit length for the conductor is as follows:

$$f_w = 0.00523DV^2 (lb/ft) (40)$$

Each conductor is considered as a catenary, as shown in Fig. 13 (a). Taking half of Conductor 1 as the object, it is subject to the resultant force of distributed wind force and weight. The resultant force is considered to be a uniformly distributed force. The maximum tension T_{max} happens at the end of the conductor, and it can be decomposed into T_{max_w} and T_{max_h} as shown in the figure. The force from the conductor to the tower F is equal to T_{max} in value but in the opposite direction. The force F can also be decomposed into two forces: F_h that is equal to T_{max_h} in value but in the opposite direction and F_w that is equal to $T_{max\ w}$ in value but in the opposite direction. F_h is trivial here as it will be canceled out by the same force coming from the conductor on the other side on the same node. F_w is the only force that needs to be considered from this conductor to the tower. As shown in Fig. 13 (b), F_w can be decomposed into a force that is in the wind direction $F_{con\ wind}$ and a force that is in the vertical direction F_{con_weight} . F_{con_wind} and F_{con_weight} are equal to the wind force and weight of the half of the conductor in Fig. 13 (a), respectively. Thus, there is no need to perform analysis of the conductor to know the force from the conductor to the tower, rendering the limit state functions for the conductors and the tower independent of each other.



(a) Conductor force diagram

(b) Force to tower

Fig. 13 Force between conductor and tower

As the tower is considered as a truss structure, the wind load on the tower is considered to be distributed to Node 1~6. The tower is divided into an upper part (consisting of all members connecting any two of Node 1~6) and a lower part (consisting of all members connecting any two of Node 3~10). For the upper part, the total wind load F_{up} is calculated using Eq. (37), (38) and (39), and the load is considered to be a wind force applied to the middle of the upper part (z =75ft). The total projected area perpendicular to the wind direction is 200 ft² (it is assumed in this study the area remains unchanged when the sizes of members change). Plugging all the numbers, the total wind load on the upper part can be calculated as follows:

$$F_{up} = 0.985V^2 (lb) (41)$$

Half of F_{up} is evenly distributed to Node 1 and 2, and the other half is evenly distributed to Node 3~6. Similarly, considering z = 25 ft and $A_f = 300 ft^2$, the total wind load on the lower part can be calculated as follows:

$$F_{low} = 1.172V^2 \ (lb) \tag{42}$$

 $F_{low}=1.172V^2~(lb)$ (42) Half of F_{low} is evenly distributed to Node 3~6. The tower is also subject to the loads from the conductors. The loading condition of the tower is summarized in Table 7. The displacement of the tower is calculated using structural matrix analysis.

Table 7 L	oad condition	of the tower
-----------	---------------	--------------

Node	x direction (lb)	z direction (lb)
1	$F_{up}/4 + 2F_{con_wind}$	$-2F_{con_weight}$
2	$F_{up}/4 + 2F_{con_wind}$	$-2F_{con_weight}$
3	$F_{up}/8 + F_{low}/8$	0
4	$F_{up}/8 + F_{low}/8$	0
5	$F_{up}/8 + F_{low}/8$	0
6	$F_{up}/8 + F_{low}/8$	0

The objective function to minimize is the total cost of the tower and the conductors. For each conductor, only half of the conductor is considered to be in the system. The costs considered herein are 10 \$\int \text{in}^3\$ for both conductors and the tower. The initial design point $[A_{10}, A_{20}, ..., A_{60}, CD_0]^T$ is set as $[0.4, 0.4, 3.4, 1.3, 0.9, 1, 0.125]^T$.

$$find. \ \boldsymbol{\mu_x} = \begin{bmatrix} \mu_{A_1}, \mu_{A2}, \mu_{A_3}, \mu_{A_4}, \mu_{A_5}, \mu_{A_6}, \mu_{CD} \end{bmatrix}^T$$

$$min. \ Total \ cost \ of \ the \ tower \ and \ conductor$$

$$\begin{cases} Pr(g_{tower}(A_1, A_2, ..., A_6, CD, V, E) < 0) \leq \Phi(-\beta_1^t), & \beta_1^t = 2, \\ Pr(g_{conductor}(CD, V) < 0) \leq \Phi(-\beta_2^t), & \beta_2^t = 2, \\ 0.2 \leq \mu_{A_1} \leq 3.6, & 0.7 \leq \mu_{A_2} \leq 0.8, & 17 \leq \mu_{A_3} \leq 28, \\ 7.3 \leq \mu_{A_4} \leq 8.3, & 7.3 \leq \mu_{A_5} \leq 8.3, & 2.9 \leq \mu_{A_6} \leq 3.9, \\ 2.9 \leq \mu_{CD} \leq 3.9 \\ A_1 \sim LN(\mu_{A_1}, 0.04^2), A_2 \sim LN(\mu_{A_2}, 0.04^2), A_3 \sim LN(\mu_{A_3}, 0.34^2) \\ A_4 \sim LN(\mu_{A_4}, 0.13^2), A_5 \sim LN(\mu_{A_5}, 0.09^2), A_6 \sim LN(\mu_{A_6}, 0.1^2) \\ CD \sim LN(\mu_{CD}, 0.0125^2) \\ E \sim LN(10^7, 10^6), V \sim Gumbel(150, 15^2) \end{cases}$$

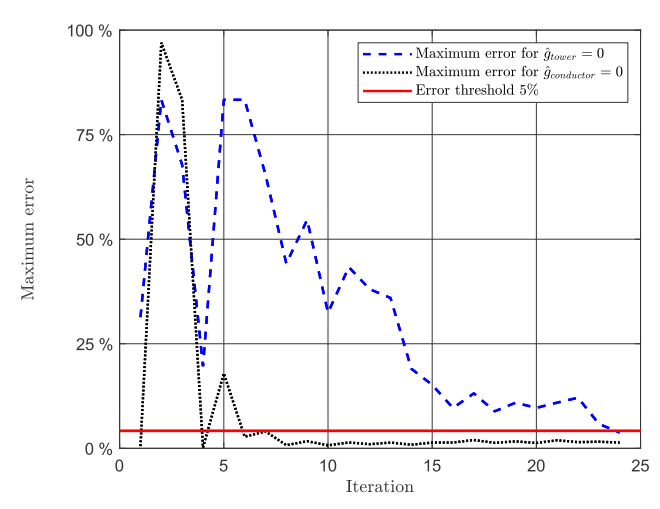


Fig. 14 Maximum error trends for the two active constraints

Table 8 Final result for Example 5

Method	Optimum	$oldsymbol{eta}_1$	$oldsymbol{eta}_2$	$N_{total}(N_{obj} + N_{con})$
Proposed	2763789 (0.2, 0.72, 3, 0.5, 0.4, 0.5, 2.3722)	2.03	2.00	108 (30+78)

Both the proposed method and the approach by Li et al. (2020) are implemented to solve the problem. The proposed method is able to reach an optimum solution with 108 total function calls including 30 for the objective function and 78 for the constraints, respectively. The solution by the proposed method is shown in Table 8. The maximum error trends for the two constraint are shown in Fig. 14. It can be observed that although the maximum error for $\hat{g}_{conductor}$ is below the threshold before the entire process ends, the relocation of the estimated optimal point re-activates the refinement of $\hat{g}_{conductor}$. At the end of the process, maximum errors for both constraint surrogate models are below the threshold. The method by Li et al. (2020) is not able to converge with even 600 total function calls and there is no sign of the solution approaching to a feasible solution or convergence. In this case where the two constraints are entirely independent of each other, sharing the training points among different constraint surrogate models used in the common Kriging-based methods can hinder the refinement of the surrogate models. In this approach, the selection of the training point in each iteration can only favor the refinement of one of the surrogate models. For other surrogate models the information from this training point can not only be uninformative, but also may have negative effects. As the process goes on, additional uninformative training points can result in ill-conditioned surrogate models, hence the difficulties in convergence. For problems that have independent constraint functions, independent training of the surrogate model can improve the efficiency and accuracy of the training significantly.

6. Conclusions

This paper proposes a quantile-based sequential method with adaptive Kriging for solving RBDO problems with independent constraint functions. In the proposed approach, Kriging surrogate models are used to replace the often computationally demanding original functions in engineering problems. The integration of an error-based stopping criterion, referred to as ESC, provides information on the error rates of the performance function surrogate models, which can be used as a measurement of the accuracy of the surrogate models for reliability estimation. This measurement is used to inform whether the surrogate models are sufficiently accurate and develop a strategy for the independent training of the models. The proposed approach thus avoids unnecessary function

evaluations in the refinement of surrogate models while ensuring their accuracy. In addition, a new sampling approach named ICBS is proposed. For each individual constraint, ICBS provides instructions on how to select training points that can improve the surrogate models for the performance functions on both deterministic and probabilistic constraints. The latter feature is often not considered when refining the surrogate models in existing methods. The performance of the proposed method is demonstrated through five RBDO problems. It is observed that for the first four typical RBDO problems, the proposed method is able to find the optimum design with significantly higher efficiency than the existing state-of-the-art methods by as much as 40%~60% under the assumption that the constraint functions are independent. The fifth example is a practical engineering problem where the constraint functions are actually independent. The proposed method is able to achieve an optimal solution, while another state-of-the-art method is not able to converge for the problem. The proposed method can be used to solve problems with independent constraint functions efficiently.

Acknowledgement

This research was supported in part by the U.S. National Science Foundation (NSF) through awards CMMI-1635569, 1762918, 2000156. Any opinions, findings, and conclusions or recommendations expressed in this paper are those of the authors and do not necessarily reflect the views of the National Science Foundation. This work was also supported in part by Lichtenstein endowment at The Ohio State University. These supports are greatly appreciated.

References

- ASCE (American Society of Civil Engineers), 2016. Minimum design loads for buildings and other structures. Standard ASCE/SEI 7-10.Reston, ,VA, USA.
- Bichon, B.J., Eldred, M.S., Mahadevan, S., McFarland, J.M., 2012. Efficient Global Surrogate Modeling for Reliability-Based Design Optimization. J. Mech. Des. 135, 011009-011009-13. https://doi.org/10.1115/1.4022999
- Bichon, B.J., Eldred, M.S., Swiler, L.P., Mahadevan, S., McFarland, J.M., 2008. Efficient global reliability analysis for nonlinear implicit performance functions. AIAA J. 46, 2459–2468.
- Blatman, G., Sudret, B., 2010. An adaptive algorithm to build up sparse polynomial chaos expansions for stochastic finite element analysis. Probabilistic Eng. Mech. 25, 183–197.
- Bourinet, J.-M., 2016. Rare-event probability estimation with adaptive support vector regression surrogates. Reliab. Eng. Syst. Saf. 150, 210–221.
- Chen, X., Hasselman, T., Neill, D., Chen, X., Hasselman, T., Neill, D., 1997. Reliability based structural design optimization for practical applications, in: 38th Structures, Structural Dynamics, and Materials Conference, Structures, Structural Dynamics, and Materials and Co-Located Conferences. American Institute of Aeronautics and Astronautics. https://doi.org/10.2514/6.1997-1403
- Chen, Z., Peng, S., Li, X., Qiu, H., Xiong, H., Gao, L., Li, P., 2015. An important boundary sampling method for reliability-based design optimization using kriging model. Struct. Multidiscip. Optim. 52, 55–70. https://doi.org/10.1007/s00158-014-1173-0
- Cho, T.M., Lee, B.C., 2011. Reliability-based design optimization using convex linearization and sequential optimization and reliability assessment method. Struct. Saf. 33, 42–50. https://doi.org/10.1016/j.strusafe.2010.05.003

- Dai, H., Zhang, H., Wang, W., Xue, G., 2012. Structural reliability assessment by local approximation of limit state functions using adaptive Markov chain simulation and support vector regression. Comput.-Aided Civ. Infrastruct. Eng. 27, 676–686.
- Darestani, Y.M., Shafieezadeh, A., Cha, K., 2020. Effect of modelling complexities on extreme wind hazard performance of steel lattice transmission towers. Struct. Infrastruct. Eng. 16, 898–915. https://doi.org/10.1080/15732479.2019.1673783
- Du, X., Chen, W., 2004. Sequential Optimization and Reliability Assessment Method for Efficient Probabilistic Design. J. Mech. Des. 126, 225–233. https://doi.org/10.1115/1.1649968
- Dubourg, V., Sudret, B., Bourinet, J.-M., 2011. Reliability-based design optimization using kriging surrogates and subset simulation. Struct. Multidiscip. Optim. 44, 673–690. https://doi.org/10.1007/s00158-011-0653-8
- Echard, B., Gayton, N., Lemaire, M., 2011. AK-MCS: an active learning reliability method combining Kriging and Monte Carlo simulation. Struct. Saf. 33, 145–154.
- Echard, B., Gayton, N., Lemaire, M., Relun, N., 2013. A combined importance sampling and kriging reliability method for small failure probabilities with time-demanding numerical models. Reliab. Eng. Syst. Saf. 111, 232–240.
- Fauriat, W., Gayton, N., 2014. AK-SYS: An adaptation of the AK-MCS method for system reliability. Reliab. Eng. Syst. Saf. 123, 137–144.
- Giunta, A.A., McFarland, J.M., Swiler, L.P., Eldred, M.S., 2006. The promise and peril of uncertainty quantification using response surface approximations. Struct. Infrastruct. Eng. 2, 175–189.
- Hasofer, A.M., Lind, N.C., 1974. Exact and Invariant Second-Moment Code Format. J. Eng. Mech. Div. 100, 111–121.
- Ho-Huu, V., Nguyen-Thoi, T., Le-Anh, L., Nguyen-Trang, T., 2016. An effective reliability-based improved constrained differential evolution for reliability-based design optimization of truss structures. Adv. Eng. Softw. 92, 48–56. https://doi.org/10.1016/j.advengsoft.2015.11.001
- Huang, X., Chen, J., Zhu, H., 2016. Assessing small failure probabilities by AK–SS: an active learning method combining Kriging and subset simulation. Struct. Saf. 59, 86–95.
- Koch, P.N., Yang, R.-J., Gu, L., 2004. Design for six sigma through robust optimization. Struct. Multidiscip. Optim. 26, 235–248. https://doi.org/10.1007/s00158-003-0337-0
- Lee, I., Choi, K.K., Zhao, L., 2011. Sampling-based RBDO using the stochastic sensitivity analysis and Dynamic Kriging method. Struct. Multidiscip. Optim. 44, 299–317. https://doi.org/10.1007/s00158-011-0659-2
- Lee, J.J., Lee, B.C., 2005. Efficient evaluation of probabilistic constraints using an envelope function. Eng. Optim. 37, 185–200. https://doi.org/10.1080/03052150512331315505
- Lee, J.-O., Yang, Y.-S., Ruy, W.-S., 2002. A comparative study on reliability-index and target-performance-based probabilistic structural design optimization. Comput. Struct. 80, 257–269. https://doi.org/10.1016/S0045-7949(02)00006-8
- Lee, T.H., Jung, J.J., 2008. A sampling technique enhancing accuracy and efficiency of metamodel-based RBDO: Constraint boundary sampling. Comput. Struct.,

- Structural Optimization 86, 1463–1476. https://doi.org/10.1016/j.compstruc.2007.05.023
- Li, G., Yang, H., Zhao, G., 2020. A new efficient decoupled reliability-based design optimization method with quantiles. Struct. Multidiscip. Optim. 61, 635–647. https://doi.org/10.1007/s00158-019-02384-7
- Li, X., Gong, C., Gu, L., Jing, Z., Fang, H., Gao, R., 2019. A reliability-based optimization method using sequential surrogate model and Monte Carlo simulation. Struct. Multidiscip. Optim. 59, 439–460. https://doi.org/10.1007/s00158-018-2075-3
- Liu, J., Cai, H., Jiang, C., Han, X., Zhang, Z., 2018a. An interval inverse method based on high dimensional model representation and affine arithmetic. Appl. Math. Model. 63, 732–743. https://doi.org/10.1016/j.apm.2018.07.009
- Liu, J., Cao, L., Jiang, C., Ni, B., Zhang, D., 2020. Parallelotope-formed evidence theory model for quantifying uncertainties with correlation. Appl. Math. Model. 77, 32–48. https://doi.org/10.1016/j.apm.2019.07.017
- Liu, J., Liu, H., Jiang, C., Han, X., Zhang, D.Q., Hu, Y.F., 2018b. A new measurement for structural uncertainty propagation based on pseudo-probability distribution. Appl. Math. Model. 63, 744–760. https://doi.org/10.1016/j.apm.2018.07.017
- Liu, J., Meng, X., Xu, C., Zhang, D., Jiang, C., 2018c. Forward and inverse structural uncertainty propagations under stochastic variables with arbitrary probability distributions. Comput. Methods Appl. Mech. Eng. 342, 287–320. https://doi.org/10.1016/j.cma.2018.07.035
- Liu, P.-L., Der Kiureghian, A., 1991. Optimization algorithms for structural reliability. Struct. Saf. 9, 161–177. https://doi.org/10.1016/0167-4730(91)90041-7
- Liu, X., Wu, Y., Wang, B., Ding, J., Jie, H., 2017. An adaptive local range sampling method for reliability-based design optimization using support vector machine and Kriging model. Struct. Multidiscip. Optim. 55, 2285–2304. https://doi.org/10.1007/s00158-016-1641-9
- Lophaven, S.N., Nielsen, H.B., Søndergaard, J., 2002a. DACE-A Matlab Kriging toolbox, version 2.0.
- Lophaven, S.N., Nielsen, H.B., Søndergaard, J., 2002b. Aspects of the matlab toolbox DACE. Informatics and Mathematical Modelling, Technical University of Denmark, DTU.
- Lv, Z., Lu, Z., Wang, P., 2015. A new learning function for Kriging and its applications to solve reliability problems in engineering. Comput. Math. Appl. 70, 1182–1197. https://doi.org/10.1016/j.camwa.2015.07.004
- Ma, L., Bocchini, P., Christou, V., 2020. Fragility models of electrical conductors in power transmission networks subjected to hurricanes. Struct. Saf. 82, 101890. https://doi.org/10.1016/j.strusafe.2019.101890
- Mourelatos, Z.P., 2005. Design of crankshaft main bearings under uncertainty, in: ANSA&mETA International Congress. Athos Kassndra, Halkidiki, Greece.
- Moustapha, M., Sudret, B., Bourinet, J.-M., Guillaume, B., 2016. Quantile-based optimization under uncertainties using adaptive Kriging surrogate models. Struct. Multidiscip. Optim. 54, 1403–1421. https://doi.org/10.1007/s00158-016-1504-4
- Pretorius, C., Craig, K., Haarhoff, J., 2004. Kriging Response Surfaces as an Alternative Implementation of RBDO in Continuous Casting Design Optimization, in: 10th AIAA/ISSMO Multidisciplinary Analysis and Optimization Conference. American

- Institute of Aeronautics and Astronautics, New York. https://doi.org/10.2514/6.2004-4519
- Ramakrishnan, B., Rao, S.S., 1996. A General Loss Function Based Optimization Procedure for Robust Design. Eng. Optim. 25, 255–276. https://doi.org/10.1080/03052159608941266
- Ramu, P., Qu, X., Youn, B.D., Haftka, R.T., Choi, K.K., 2006. Inverse reliability measures and reliability-based design optimisation. Int. J. Reliab. Saf. 1, 187–205.
- Rao, S.S., 2019. Engineering Optimization: Theory and Practice. John Wiley & Sons.
- Romero, V.J., Swiler, L.P., Giunta, A.A., 2004. Construction of response surfaces based on progressive-lattice-sampling experimental designs with application to uncertainty propagation. Struct. Saf. 26, 201–219.
- Saka, M.P., 1990. Optimum Design of Pin-Jointed Steel Structures With Practical Applications. J. Struct. Eng. 116, 2599–2620. https://doi.org/10.1061/(ASCE)0733-9445(1990)116:10(2599)
- Song, K., Zhang, Y., Zhuang, X., Yu, X., Song, B., 2019. Reliability-based design optimization using adaptive surrogate model and importance sampling-based modified SORA method. Eng. Comput. https://doi.org/10.1007/s00366-019-00884-0
- Toğan, V., Daloğlu, A.T., 2008. An improved genetic algorithm with initial population strategy and self-adaptive member grouping. Comput. Struct. 86, 1204–1218. https://doi.org/10.1016/j.compstruc.2007.11.006
- Tu, J., Choi, K.K., Park, Y.H., 1999. A New Study on Reliability-Based Design Optimization. J. Mech. Des. 121, 557–564. https://doi.org/10.1115/1.2829499
- UQLab Kriging (Gaussian process modelling) manual [WWW Document], 2017. . UQLab Framew. Uncertain. Quantif. URL http://www.uqlab.com/userguidekriging (accessed 5.13.17).
- Valdebenito, M.A., Schuëller, G.I., 2010. A survey on approaches for reliability-based optimization. https://doi.org/10.1007/s00158-010-0518-6
- Wang, Z., Shafieezadeh, A., 2019. REAK: Reliability analysis through Error rate-based Adaptive Kriging. Reliab. Eng. Syst. Saf. 182, 33–45. https://doi.org/10.1016/j.ress.2018.10.004
- Wang, Z., Shafieezadeh, A., 2018. ESC: an efficient error-based stopping criterion for kriging-based reliability analysis methods. Struct. Multidiscip. Optim. https://doi.org/10.1007/s00158-018-2150-9
- Wu, Y.-T., 1994. Computational methods for efficient structural reliability and reliability sensitivity analysis. AIAA J. 32, 1717–1723. https://doi.org/10.2514/3.12164
- Wu, Y.-T., Millwater, H.R., Cruse, T.A., 1990. Advanced probabilistic structural analysis method for implicit performance functions. AIAA J. 28, 1663–1669. https://doi.org/10.2514/3.25266
- Wu, Y.-T., Shin, Y., Sues, R., Cesare, M., 2001. Safety-factor based approach for probability-based design optimization, in: 19th AIAA Applied Aerodynamics Conference, Fluid Dynamics and Co-Located Conferences. American Institute of Aeronautics and Astronautics. https://doi.org/10.2514/6.2001-1522
- Yang, R.J., Gu, L., 2004. Experience with approximate reliability-based optimization methods. Struct. Multidiscip. Optim. 26, 152–159. https://doi.org/10.1007/s00158-003-0319-2

- Yi, P., Zhu, Z., Gong, J., 2016. An approximate sequential optimization and reliability assessment method for reliability-based design optimization. Struct. Multidiscip. Optim. 54, 1367–1378. https://doi.org/10.1007/s00158-016-1478-2
- Youn, B.D., Choi, K.K., Park, Y.H., 2003. Hybrid Analysis Method for Reliability-Based Design Optimization. J. Mech. Des. 125, 221–232. https://doi.org/10.1115/1.1561042
- Zhang, C., Wang, Z., Shafieezadeh, A., 2020. Value of Information Analysis via Active Learning and Knowledge Sharing in Error-Controlled Adaptive Kriging. IEEE Access 8, 51021–51034. https://doi.org/10.1109/ACCESS.2020.2980228
- Zhao, W., Fan, F., Wang, W., 2017. Non-linear partial least squares response surface method for structural reliability analysis. Reliab. Eng. Syst. Saf. 161, 69–77. https://doi.org/10.1016/j.ress.2017.01.004
- Zhuang, X., Pan, R., 2012. A Sequential Sampling Strategy to Improve Reliability-Based Design Optimization With Implicit Constraint Functions. J. Mech. Des. 134, 021002-021002-10. https://doi.org/10.1115/1.4005597